axioms

MDPI

Article

Convergent Radiation Algorithm for Multi-Attribute Group Decision-Making with Circular Intuitionistic Fuzzy Numbers

Xiqi Li [1], Junda Qiu [1,2,*], Jiali Tang [1], Jie Zhang [1], Qi Liu [1], Taiji Li [1] and Yongjie Guo [1]

[1] School of Computer Engineering, Jiangsu University of Technology, Changzhou 213001, China; 2025605017@smail.jsut.edu.cn (X.L.); tangjl@jsut.edu.cn (J.T.); zhangjie@jsut.edu.cn (J.Z.); qi.liu@jsut.edu.cn (Q.L.); 2025605016@smail.jsut.edu.cn (T.L.); 2025605018@smail.jsut.edu.cn (Y.G.)
[2] School of Electrical Engineering, Southeast University, Nanjing 210096, China
* Correspondence: qiujd@jsut.edu.cn

Abstract

This paper proposes a novel method, the Convergent Radiation Algorithm (CRA), aimed at multi-attribute group decision-making (MAGDM) in circular intuitionistic fuzzy settings. The approach is aimed at reaching geometric consensus among experts, with uncertainties and hesitancies expressed via circular intuitionistic fuzzy numbers (CIFNs). First, the qualitative judgment in professionals is converted into a geometric space where experts' assessments are represented as spatial points that reflect the differences between the opinions. All these points are gradually combined with the help of a radiation–reflection–convergence mechanism, which iteratively finds the Optimal Consensus Point (OCP) to minimize the overall weighted divergence over the evaluations. After that, a projection-based scoring method is used to locate good and bad optimal solutions, and the alternatives are ranked based on a comparison of their projection distance. It presents a numerical example with data supplied by the Hubei agro-ecological zone to demonstrate that the offered method helps to capture collective agreement and convergence behavior that is consistent, and makes the decision results readable and reliable.

Keywords: multi-attribute group decision-making (MAGDM); circular intuitionistic fuzzy numbers (CIFNs); convergent radiation algorithm (CRA); optimal consensus point (OCP); projection-based scoring

MSC: 90B50

Check for updates

Academic Editor: Manuel Arana-Jimenez

Received: 19 December 2025
Revised: 15 January 2026
Accepted: 22 January 2026
Published: 26 January 2026

Copyright: © 2026 by the authors. Licensee MDPI, Basel, Switzerland. This article is an open access article distributed under the terms and conditions of the Creative Commons Attribution (CC BY) license.

1. Introduction

Since Zadeh's pioneering work in the field of fuzzy set theory [1], uncertainty models have become a key foundation for multi-attribute group decision-making (MAGDM). They possess the ability to present human judgment, hesitation, and imprecision within an irregular mathematical framework, and this ability has largely transformed decision science. Over the past few decades, a number of extended contents have been proposed to enhance the descriptive and operational capabilities of fuzzy systems. Intuitionistic fuzzy sets and Pythagorean fuzzy sets provided early methods for representing membership and non-membership degrees, while q-rung orthopair fuzzy sets have generalized these models. They have made significant improvements in information representation and tolerance for high uncertainty, offering greater flexibility in modeling the interaction between membership and non-membership degrees as well as in accommodating heterogeneous expert opinions. Recently, circular intuitionistic fuzzy sets (C-IFSs) have

emerged, providing a geometric interpretation of uncertainty. Under this representation, experts' evaluations are expressed as points within a circular domain rather than scalar values on a linear continuum. This geometric embedding enables the dependence between membership and non-membership to be explicitly constrained and coherently quantified, thereby enhancing modeling flexibility in representing uncertainty structures. These advancements have stimulated the emergence of many decision-making models, such as the circular intuitionistic fuzzy sorting and allocation framework [2,3], the Einstein–Bonferroni operator in Fermatean hesitant fuzzy environments [4], and hybrid methods integrating language, probability, or q-rung orthopair fuzzy information [5–7]. Overall, these developments illustrate how fuzzy expansion is constantly evolving towards high-dimensional and information-rich representations, which enhance computational adaptability and also improve the ability to explain reality in the decision-making process.

Among recent contributions, the study by Chen [8]—hereafter the ORESTE-CIF model—offers a systematic framework for MAGDM under circular intuitionistic fuzzy environments. The ORESTE-CIF model introduces a projection-driven ranking mechanism, which can map the expert's evaluation content into a multi-dimensional fuzzy space. It is also allowed to determine the quantitative method for reaching a consensus by means of geometric approximation. This research achievement demonstrates how projection-based modeling methods can capture the potential relationships between expert evaluations while ensuring interpretability and computational traceability. However, although this method seems rather complex, the ORESTE-CIF model and similar project-driven models still face three challenges that have not been solved in the MAGDM literature until now.

Firstly, there is a heavy reliance on preprocessing. Currently, most decision-making frameworks still rely on entropy-based weighting schemes [9], similarity transformations [10], and distance-based standardization procedures [11]. Before aggregating heterogeneous data, these data are normalized. Although such transformations do indeed improve the comparability of numerical values, they also make the calculation more stable, but at the same time, they change the original intrinsic geometric structure of the data. This means that some subtle changes in expert evaluations may disappear during the repetitive normalization or scaling process, as reflected in the probability-weighted sum bidirectional projection formula of the Fermatean hesitant fuzzy environment, which demonstrates [12] the continuous efforts of people to improve the accuracy of fuzzy measurement. However, these methods still rely on pre-set distance metrics or normalization constraints. As a result, any process that aims to reduce information bias may bring about new distortions and alter the semantic relationships among expert opinions. Theoretically speaking, this reliance on preprocessing conflicts with a core of the fuzzy model. This core objective is to preserve the natural structure of human uncertainty. Nowadays, there is an increasing need for aggregation methods that can directly handle raw or minimally processed fuzzy data. This can reduce external interference and also ensure the authenticity of experts' cognition.

The second challenge is brought about by the overuse and central dominance of aggregation operators. Weighted averages and their variants still hold a dominant position in the literature due to their simplicity, explainability, and ease of implementation [13], although various eye-catching operators have been proposed, like those of Hamacher, Frank, Dombi, Einstein, Hamy, and Heronianhas, which are used to deal with different decision-making environments [14–16], but their structural behaviors are basically of an algebraic nature. Most of these methods assume that the opinions of experts are commensurable and can be linearly fused through parametric operators. However, in actual situations, the judgments of experts are rarely the same. They differ in terms of accuracy, confidence, and interpretation of attributes. A unified operator is used to summarize all inputs. It may inadvertently mask the very prominent cognitive diversity

among decision-makers. Once the operator is selected, the parameters it embeds often determine the final decision-making trend. As a result, the space for adaptive adjustment is very limited. This phenomenon is sometimes called operator-led, which means that the decision-making outcome may more reflect the operator's design rather than the actual expert reasoning. A new method is needed to clearly capture how the heterogeneity of the experts' models' interpersonal differences and promote data-driven consensus rather than formulaic consensus. This approach should emphasize geometric or structural integration rather than merely algebraic averaging, allowing group consensus to arise naturally from the relationships among experts.

The third limitation is related to the convergence of the algorithmic convergence and solution stability. Even if the algorithm framework incorporates advanced optimization mechanisms, they often encounter the problem of converging prematurely to local optima in high-dimensional or nonlinear fuzzy environments. Recent studies have demonstrated improvements in interpretability and efficiency by leveraging projection-based similarity measures [12], circular intuitionistic fuzzy preference relations [17], and consensus-reaching processes [18]. However, these methods still rely on fixed update rules and deterministic search paths, which limits their ability to explore the global solution space. Similarly, conflict elimination strategies based on opinion dynamics improve numerical stability, but they often lock the system in local equilibrium. Once the consensus threshold is reached, it is impossible to optimize. This problem of premature stability indicates that the existing convergence schemes do not have sufficient adaptability to capture the nonlinear feedback mechanism that can represent the deliberation of real-world groups. A robust decision-making algorithm should integrate dynamic search control, balance exploration and development, and allow the solution path to be adjusted according to the evolution of the divergence structure.

From the above content, it can be seen that the three issues of preprocessing dependency, operator dominance, and premature convergence actually reveal a fundamental deficiency in current MAGDM research: there is currently a lack of a unified and adaptive framework that can integrate the original expert information, geometric diversity, and iterative global optimization. Under such circumstances, this paper introduces the Convergent Radiation Algorithm (CRA) in a circular intuitionistic fuzzy environment, namely CRA. CRA redefines the aggregation process as the radiative convergence dynamics in the information-energy domain. In this dynamic process, expert evaluations rely on iterative steps of radiation, reflection, and convergence to interact with each other. By relying on the simulation of how information spreads outward and then converges back to a balanced state, the CRA system can systematically determine a globally stable consensus, which is called the Optimal Consensus Point, or OCP. This geometric mechanism is fundamentally different from the traditional operator-based fusion. The reason lies in the fact that it regards each expert's input as an energy particle that affects the collective balance, rather than a weight in the formula. This algorithm avoids stagnation at an early stage by adaptively adjusting the search direction and step size, and continuously explores new solution trajectories until the global energy is minimized. CRA reduces its reliance on preprocessing [19], which refers to the reference and utilizes weighted spatial dispersion [20]. That is, as discussed in [21], the proposed mechanism explicitly simulates the thermal erosion of expert opinions and introduces a self-regulating feedback process, which effectively reduces the risk of local convergence. In this way, the method integrates geometric optimization with consensus formation, providing a flexible and theoretically grounded paradigm for robust multi-attribute group decision-making.

2. Related Work

This section reviews representative studies related to circular intuitionistic fuzzy group decision-making and projection-based aggregation methods. Particular attention is paid to existing aggregation frameworks that emphasize similarity measurement, operator-driven fusion, and convergence mechanisms, as well as their respective advantages and limitations. Based on this review, the motivation for developing a geometry-oriented consensus aggregation strategy is further clarified.

2.1. Objectives of the Study

Motivated by the limitations identified in existing circular intuitionistic fuzzy group decision-making frameworks, the objectives of this study are threefold. First, this work aims to develop a geometry-oriented aggregation mechanism that can directly operate on circular intuitionistic fuzzy information while preserving its intrinsic geometric structure, thereby reducing information distortion caused by excessive preprocessing. Second, the study seeks to design a deterministic consensus-search strategy capable of achieving stable convergence toward a global equilibrium, even under heterogeneous and multimodal expert opinion distributions. Third, this paper aims to establish an interpretable projection-based evaluation framework that integrates naturally with the proposed aggregation process and provides reliable and transparent ranking results for multi-attribute group decision-making problems.

The above objectives jointly guide the methodological design of the proposed Convergent Radiation Algorithm and serve as the basis for the comparative analysis presented in the subsequent sections.

2.2. Contributions and Limitations of the ORESTE-CIF Model

Group-based aggregation frameworks have received increasing attention in the past few years as researchers have attempted to balance expert diversity with collective consistency. Among these, the study by Chen [8], hereafter referred to as the ORESTE-CIF model, represents one of the most systematic and influential contributions to multi-attribute group decision-making (MAGDM) under circular intuitionistic fuzzy environments. The ORESTE-CIF framework introduced a projection-driven similarity mechanism that maps expert evaluations into a multidimensional fuzzy space, allowing a quantitative measure of consensus through geometric proximity. This contribution demonstrated how projection-based modeling can capture latent relations between experts' evaluations while maintaining interpretability and computational tractability. Similar modeling paradigms can be observed in recent research on hybrid ranking systems [22], projection-based similarity under hesitant or intuitionistic fuzzy environments [23], and Pythagorean or q-rung orthopair extensions to distance/measure families [24], as well as projection-style TOPSIS and metric refinements in circular or intuitionistic settings [25]. All these works have a methodological basis that can be compared with each other. They rely on projection measurements or distance-driven operators to obtain collective results under uncertain conditions.

However, although these methods are rather complex, models like the ORESTE-CIF often exhibit some structural limitations. The first aspect is that they particularly rely on information preprocessing, such as normalization, entropy-based reweighting, or similarity transformation, which may make the relationships between the original data less clear. The second aspect is that they rely on pre-defined operators and linear aggregation mechanisms to compress the judgments of different experts into a single prime. This way, the diversity of cognition is overlooked. The third aspect is that their iterative processes generally adopt a step-convergence scheme, which may stabilize prematurely before reaching the global optimal consensus. Among these methods, the ORESTE-CIF model is particularly

representative because it integrates the three features of comprehensive data preprocessing, operator-driven aggregation, and projection-based convergence within a unified framework. It provides a meaningful benchmark for evaluating the inherent trade-offs among interpretability, flexibility, and algorithmic depth, and can also be regarded as a diagnostic case. Considering that the ORESTE-CIF model concept is relatively complete, it has been widely used in recent decision analyses. This paper selects the ORESTE-CIF model as the main comparison baseline for subsequent evaluation and algorithm verification.

2.3. Preprocessing Dependence and Information Distortion

To ensure that data can be compared and to facilitate the smooth progress of calculations, preprocessing has always been regarded as an indispensable step in MAGDM. Entropy weights [26] and distance normalization [27] are often used to eliminate scale differences, while similarity adjustments [28] can help reach consensus among experts within the same evaluation framework. However, a large amount of preprocessing adds an artificial layer between the expert's judgment and the representation of calculation. Each transformation, whether it is normalization, defuzzification, or weighting, inevitably changes the underlying geometry of the fuzzy evaluation. Take the ORESTE-CIF framework as an example. Entropy-based normalization is carried out before the aggregation process. The shape and scale of the circular intuitionistic fuzzy domain were changed before the implementation of the similarity projection. In this way, some of the inherent uncertain structures in the original expert matrix will be lost or distorted, reducing the fidelity of the explanation.

To solve this problem, this study adopted a geometric strategy, that is, relying on the CRA to directly aggregate the original fuzzy data without the need for extensive preprocessing. In the CRA framework, each expert's evaluation is regarded as an energy particle embedded in the information energy field. This algorithm does not transform data through statistical weighting but minimizes the overall energy dispersion among experts to find a collective equilibrium state. This mechanism normalizes the differences among experts during the optimization process. Instead of doing it before optimization, the original topological structure of the decision space is retained. CRA can achieve scale-free convergence, which makes it particularly suitable for multi-expert systems with significant differences in attribute weights, evaluation intervals, or uncertainty radii. With such a design, CRA reduces information distortion and maintains a high level of semantic transparency between human judgment and algorithmic calculation.

2.4. Algorithmic Convergence and Local Optima Risks

In the existing MAGDM literature, there is a frequently occurring limitation, which is the tendency of premature convergence. Traditional algorithms that rely on projection and consensus generally adopt a deterministic iterative scheme. In this scheme, the update direction and step size of the iteration remain unchanged. In this fixed setting, most of the time, the optimized trajectory will fall into a local optimum or boundary equilibrium. Although recent methods that adopt adaptive preference relations [29] or dynamic opinion adjustment [19] have improved stability, they generally explore the decision space in a linear or sequential manner, which limits their ability to explore in multiple directions. The ORESTE-CIF framework itself adopts a similar-driven convergence criterion. Once the aggregated projection distance is lower than the fixed threshold, this criterion will stop. Although this approach is quite efficient in calculation, this fixed convergence boundary hinders the exploration of the solution space when the opinions of experts present a multimodal distribution.

The CRA has embedded adaptability in the optimization process, fundamentally changing this convergence paradigm. It models the search dynamics as a radiation–reflection–convergence cycle: At the very beginning, it radiates from the initial consensus center in multiple different directions, then reflects back from the local energy peak. This way, it can avoid being trapped, and finally converges again towards the global equilibrium, which is also called the OCP. By introducing an adaptive step size mechanism, CRA can dynamically balance exploration and development. If improvement comes to a standstill, the search radius is expanded; if it approaches a balanced state, the search radius is reduced. This radiation mechanism can prevent premature stabilization and ensure that consensus is reached through global optimization rather than local optimization. Because CRA assesses progress by means of an information-energy-potential function rather than a fixed-distance metric, it can capture convergence and divergence nonlinear patterns more accurately than traditional projection or entropy-based methods. The final result is that the convergence curve will be smoother, the reproducibility will be higher, and the resistance to local minima will be significantly improved.

2.5. Research Gap and Directions for Improvement

The above analysis highlights a situation that frequently occurs in the recent development of MAGDM: Most of the current frameworks either sacrifice the integrity of information for the sake of prioritizing computational convenience or rely on fixed iterative schemes, which limit global exploration. Although projection-based models like the ORESTE-CIF framework can provide interpretability and mathematical consistency, in complex decision-making environments, they lack the adaptability and flexibility needed to simulate the interaction among heterogeneous experts. Conversely, operator-based systems can effectively integrate inputs, but most of the time, they blur the divergent structures that are crucial for forming meaningful consensus. There is a particular need for a method that can combine the interpretability of the projection model, the adaptability of the optimization algorithm, and the reality of geometric aggregation.

The CRA proposed in this study directly resolves this issue, integrating all the advantages mentioned above into a single framework. Its contribution can be discussed from three interrelated aspects. CRA uses geometric energy optimization instead of statistical preprocessing, thus preserving the structure of the circular intuitionistic fuzzy evaluation itself and keeping the explanation transparent and clear. CRA introduces a radiation–reflection convergence mechanism, which can dynamically adjust the direction and step size of the search. Enable the system to break away from the local minimum and eventually converge to the Optimal Consensus Point. CRA has constructed a collective decision-making matrix based on energy dispersion minimization, which naturally incorporates the heterogeneity among experts into the consensus results, achieving individual fairness and group consistency. Compared with existing methods, this approach has stronger robustness, faster convergence speed, and can also ensure better consistency among expert groups. CRA supplements the advantages of projection-based clustering and expands its theoretical scope, providing a new foundation for robust and interpretable multi-attribute group decision-making.

3. Preliminaries

3.1. Foundational Concepts of Preference Relations

In the process of multi-attribute group decision-making, or MAGDM for short, the preference relationship is actually the basis for expressing the criticality of one alternative compared to another. Every decision-maker compares alternatives in a pairwise manner, thereby forming a fuzzy preference relation (FPR). Relevant studies like [30] particularly

emphasize that even if the complexity of the model increases, FPR remains the structure that can be most clearly explained and is relatively stable in terms of calculation among expert opinions.

$$Z = \{z_1, z_2, \ldots, z_n\}, \quad n \geq 2. \tag{1}$$

A fuzzy preference relation $Q = (q_{ij})_{n\times n}$ is defined as a mapping

$$\mu_Q : Z \times Z \to [0,1], \tag{2}$$

where each entry q_{ij} denotes the degree to which z_i is preferred to z_j. If $q_{ij} = 0.5$, the two alternatives are considered equally preferable.

Such fuzzy preference relations have been extensively studied as a fundamental representation of pairwise comparisons in group decision-making [31,32].

A key property of FPRs is *additive consistency* (also referred to as additive transitivity). For an additively reciprocal FPR satisfying $q_{ij} \in [0,1]$, $q_{ii} = 0.5$, and $q_{ij} + q_{ji} = 1$, additive consistency can be expressed as

$$q_{ij} + q_{jk} + q_{ki} = 1.5, \qquad \forall i, j, k \in \{1, \ldots, n\}. \tag{3}$$

Equivalently, it can be written as $q_{ij} = q_{ik} + q_{kj} - 0.5$, which has been widely used to ensure transitive coherence in fuzzy preference relations [31,33].

This condition guarantees that indirect preferences derived from $i \to j \to k$ correspond to the direct preference between i and k.

When an FPR is inconsistent, it can be transformed into an additively consistent relation $T = (t_{ij})$ using a classical adjustment operator proposed in the fuzzy preference literature:

$$t_{ij} = \frac{1}{2} + \frac{1}{n}\left(\sum_{k=1}^{n} q_{ik} - \sum_{k=1}^{n} q_{jk}\right). \tag{4}$$

This transformation recalibrates pairwise judgments according to the overall preference tendency of each alternative and has been widely adopted in consistency-improving procedures [33,34]. Extensions of this operator to uncertain or radius-based fuzzy environments have been recently investigated to enhance robustness in multi-expert settings [35].

3.2. Intuitionistic and Circular Intuitionistic Fuzzy Sets (C-IFSs)

This subsection follows recent developments on circular intuitionistic fuzzy modeling and adopts the C-IFS framework as the geometric basis for representing uncertainty in a circular region around an intuitionistic point [35,36], and we restate below the IFS preliminaries and the C-IFS extension used throughout this paper.

While classical fuzzy sets include only membership information, intuitionistic fuzzy sets (IFSs) introduce a complementary non-membership degree to capture hesitation and uncertainty. Let A be an IFS on Z:

$$A = \{\langle z, \mu_A(z), \nu_A(z)\rangle \mid z \in Z\}. \tag{5}$$

where $\mu_A(z), \nu_A(z) \in [0,1]$ represent membership and non-membership degrees, satisfying

$$0 \leq \mu_A(z) + \nu_A(z) \leq 1. \tag{6}$$

The hesitancy degree $\pi_A(z)$ is given by

$$\pi_A(z) = 1 - (\mu_A(z) + \nu_A(z)). \tag{7}$$

These parameters jointly describe the balance between belief, disbelief, and hesitation.

C-IFSs extend IFSs by representing uncertainty within a circular geometric region rather than a single point. A C-IFS is defined as

$$A = \{\langle z, \mu_A(z), \nu_A(z); r_A(z)\rangle \mid z \in Z\}. \tag{8}$$

where $r_A(z) \in [0,1]$ denotes the radius of the circular region centered at $(\mu_A(z), \nu_A(z))$. Unlike the classical IFS constraint $\mu_A(z) + \nu_A(z) \leq 1$, which defines a triangular feasible region, C-IFS adopts a circular geometric constraint given by

$$\mu_A(z)^2 + \nu_A(z)^2 \leq 1. \tag{9}$$

This squared-sum formulation explicitly characterizes the unit disk in the (μ, ν) plane and serves as the geometric foundation of circular intuitionistic fuzzy modeling.

A larger radius indicates greater vagueness in expert judgment, and as $r_A(z) \to 0$, Equation (8) reduces to the classical IFS. This circular representation enhances the continuity of fuzzy mappings and provides a geometric foundation for optimization-based aggregation approaches.

3.3. Circular Intuitionistic Fuzzy Preference Relations (C-IFPRs)

Combining circular intuitionistic fuzziness with preference relations yields the C-IFPR. This structure simultaneously represents preference strength, uncertainty, and circular geometry, offering greater expressiveness than classical intuitionistic relations [17].

Let $A = (a_{ij})_{n\times n}$ denotes a C-IFPR, where

$$a_{ij} = (\mu_{ij}, \nu_{ij}; r_{ij}), \quad i, j = 1, \ldots, n,$$

represents the circular intuitionistic preference value (C-IFPV) of alternative z_i over z_j. Each element satisfies

$$\begin{cases} 0 \leq \mu_{ij} + \nu_{ij} \leq 1, \\ \mu_{ij} = \nu_{ji}, \quad \nu_{ij} = \mu_{ji}, \\ \mu_{ii} = \nu_{ii} = 0.5. \end{cases} \tag{10}$$

These conditions ensure reciprocity and self-consistency. The hesitancy and geometric distance functions are

$$\pi_{ij} = 1 - (\mu_{ij} + \nu_{ij}), \qquad d_{ij} = \sqrt{\mu_{ij}^2 + \nu_{ij}^2}. \tag{11}$$

The complement of a C-IFPV is defined as

$$a_{ij}^c = (\nu_{ij}, \mu_{ij}; r_{ij}). \tag{12}$$

Several aggregation operations have been developed for C-IFPRs. A commonly used probabilistic-sum-type addition operator is

$$a_{ij} \oplus a_{kl} = \left(\mu_{ij} + \mu_{kl} - \mu_{ij}\mu_{kl},\ \nu_{ij}\nu_{kl};\ \max(r_{ij}, r_{kl})\right). \tag{13}$$

This operator merges two preference values while preserving the dominant uncertainty radius. Such operators form the algebraic basis for the aggregation process [13].

3.4. Similarity and Entropy on CIFN Triplets

Building on the distance-to-similarity paradigm for single-valued neutrosophic environments proposed by Dasan et al. [37] and the information-theoretic entropy design for circular intuitionistic fuzzy sets introduced by Alreshidi et al. [38], we formalize the similarity $S(\cdot,\cdot)$ and the entropy $E(\cdot)$ on CIFN-embedded triplets (μ,ν,r).

Setting. Let A_i and B_i be two alternatives evaluated on n attributes, with entries $a_{ij} = (\mu_{ij}, \nu_{ij}; r_{ij})$ and $b_{ij} = (\mu'_{ij}, \nu'_{ij}; r'_{ij}) \in [0,1]^3$. All component values are bounded in $[0,1]$; the notation is consistent with the (μ,ν,r) embedding of CIFNs used throughout this paper.

Similarity(distance-to-similarity). Following a classical principle in similarity theory that a (normalized) distance can be transformed into a similarity by a monotone decreasing mapping, typically by complementing from unity [1,39], we adopt the attribute-averaged normalized Hamming distance and define This distance-to-similarity construction has also been adopted in recent neutrosophic decision models, including the single-valued neutrosophic framework of Dasan et al. [37].

$$S(A_i, B_i) = 1 - \frac{1}{n}\sum_{j=1}^{n} \frac{|\mu_{ij} - \mu'_{ij}| + |\nu_{ij} - \nu'_{ij}| + |r_{ij} - r'_{ij}|}{3}, \qquad S \in [0,1]. \tag{14}$$

Notes. (i) The factor $1/3$ normalizes the per-attribute dissimilarity to $[0,1]$. (ii) $S = 1$ if and only if $a_{ij} \equiv b_{ij}$ for all j; S decreases monotonically with component-wise deviations.

Entropy(information-theoretic). In line with Alreshidi et al. [38], the intrinsic uncertainty of A_i over (μ,ν,r) is quantified by a Shannon-type triadic entropy, averaged over attributes and normalized to $[0,1]$ (with the convention $0 \ln 0 := 0$):

$$E(A_i) = \frac{1}{n}\sum_{j=1}^{n}\left(-\frac{\mu_{ij}\ln\mu_{ij} + \nu_{ij}\ln\nu_{ij} + r_{ij}\ln r_{ij}}{\ln 3}\right), \qquad E \in [0,1]. \tag{15}$$

Notes. (i) $\ln 3$ ensures that the maximum entropy is 1 at $(\mu,\nu,r) = (\frac{1}{3},\frac{1}{3},\frac{1}{3})$. (ii) For numerical stability, evaluate $\ln(\max\{\varepsilon, x\})$ with $\varepsilon \approx 10^{-12}$.

Usage in this paper. Equation (14) is employed to assess inter-matrix agreement in the methodology section and throughout the experiments; Equation (15) is revisited alongside the (μ,ν,r) projection-based scoring as an uncertainty-aware complement (see the dedicated subsection on projection-based scoring in Section 4.6).

3.5. Recent Advances and Transition to CRA

Recent works have demonstrated the effectiveness of circular intuitionistic models in decision analysis [13,35]. By embedding fuzzy information into a circular geometric space, these studies achieve smoother aggregation and stronger interpretability. The study by Khan et al. [17] further developed a consensus-reaching mechanism using entropy weighting under the C-IFPR environment.

Despite these advances, two main challenges persist.

1. Dependence on iterative consensus processes.
   Many existing C-IFPR-based models achieve consensus through repeated matrix adjustments driven by entropy reweighting or preference propagation. Although effective in moderately sized problems, such iterative schemes often rely on fixed stopping thresholds and may converge prematurely when expert opinions exhibit multimodal or polarized distributions [33]. In such cases, the resulting consensus may reflect a numerically stable state rather than a globally representative agreement.
2. Lack of direct geometric optimization. Most current aggregation methods operate in an algebraic manner, combining preference values through averaging or operator-based fusion without explicitly modeling the spatial distribution of expert opinions.

As a result, these approaches may fail to capture the geometric structure of the decision space, particularly when expert evaluations form multiple clusters or non-convex patterns [23]. This limitation can lead to consensus outcomes that are difficult to interpret geometrically and that do not correspond to an optimal point in the underlying fuzzy space.

To illustrate this issue, consider a situation where expert evaluations form two well-separated clusters in the circular intuitionistic fuzzy domain. An algebraic aggregation may produce a compromise solution located between the clusters, even though no expert supports this position explicitly. From a geometric perspective, such a result is suboptimal, as it ignores the spatial configuration of opinions and the associated energy dispersion.

To overcome these issues, the present research introduces the CRA, a deterministic geometric optimization framework that explicitly treats expert evaluations as points in a circular fuzzy space. By minimizing a global information-energy objective, CRA performs direct spatial optimization to locate the OCP, achieving faster convergence and improved robustness to expert diversity compared with entropy-driven iterative schemes [17].

3.6. Summary

This section establishes the theoretical basis for the subsequent methodology. It defines fuzzy and circular intuitionistic preference structures, presents similarity and entropy measures, and clarifies their linkage to the four evaluation indicators used in the CRA framework. These preliminaries provide the mathematical foundation for developing the CRA-based aggregation and projection scoring system in Section 4.

4. Methodology

Building on preliminaries, which established the circular intuitionistic fuzzy (C-IF) representation and the feasible domain Ω, this section develops a deterministic geometric optimization model for MAGDM under C-IF environments. We propose a coordinate-based CRA that treats aggregation as energy minimization inside the circular domain. Unlike stochastic or multi-beam variants, the implementation used in this work is a *single-beam*, *axis-aligned* scheme designed for reproducibility and faithful alignment with the C-IF constraints. The use of feasibility projection and information-based scoring aligns with the latest developments in probabilistic linguistic consensus modeling [40] and circular intuitionistic fuzzy preference aggregation [17], ensuring theoretical consistency with modern fuzzy decision paradigms [13].

4.1. Conceptual Motivation

Traditional aggregation mechanisms in MAGDM often rely on linear averaging or static operator fusion. Such methods treat expert evaluations as isolated numeric entries rather than structured points in a constrained fuzzy geometry, which may distort the interplay among membership (μ), non-membership (ν), and reliability (r). CRA reconceives aggregation as a geometric energy-minimization process: expert opinions are seen as points that jointly induce an *information energy field* over the feasible domain. A deterministic radiation–convergence mechanism explores axis-aligned directions and iteratively reduces total disagreement until a stable equilibrium is reached. This offers three benefits: (i) geometric interpretability (movements have spatial meaning), (ii) feasibility by construction (projection enforces the C-IF constraints), and (iii) reproducibility (determinism with fixed step).

4.2. Optimal Consensus Point (OCP)

The OCP represents the geometric equilibrium of all expert evaluations under a given attribute–alternative cell. Intuitively, each expert point exerts an attraction proportional to its credibility, and the OCP is the lowest-energy position balancing all these forces in the circular intuitionistic fuzzy (C-IF) space. Formally, for expert vectors $p_{ijk} = (\mu_{ijk}, \nu_{ijk}, r_{ijk}) \in \Omega$ provided by K experts $(k = 1, \ldots, K)$, and their normalized credibilities γ_k,

$$x_{ij}^{*} = \arg\min_{x \in \Omega} f_{ij}(x), \tag{16}$$

$$f_{ij}(x) = \sum_{k=1}^{K} \gamma_k \left\| W_j (x - p_{ijk}) \right\|_2. \tag{17}$$

In Equation (17), W_j denotes a general attribute-wise weighting matrix. In the present implementation, we set $W_j = I_3$, implying that no attribute reweighting is performed during the aggregation stage. Attribute weights are instead incorporated exclusively in the projection-based scoring stage described in Section 4.6.

The function $f_{ij}(x)$ aggregates the weighted Euclidean distances from a candidate point x to all expert evaluations, and minimizing f_{ij} yields the consensus point for the cell (i, j). Although the Euclidean distance is adopted in this study for its geometric interpretability and numerical stability, the proposed framework is not restricted to this choice and can be readily extended to other distance metrics, such as Manhattan or Mahalanobis distances, depending on the underlying decision context. This process ensures that the OCP lies within the feasible circular domain Ω, where (μ, ν, r) jointly describe membership, non-membership, and reliability.

Figure 1 provides a planar explanation of the consensus process, in which each expert evaluation is represented as a point embedded in the circular intuitionistic fuzzy space and can be intuitively interpreted as a light source whose intensity is weighted by the corresponding expert credibility. The red center point $P^{*}(a^{*}, b^{*})$ denotes the Optimal Consensus Point, where the overall potential energy induced by all expert evaluations reaches its minimum. This point represents a geometrically balanced equilibrium state, indicating that heterogeneous expert opinions have converged toward a common and stable consensus.

In order to promote this concept more widely, Figure 2 expands the OCP into the three-dimensional (μ, ν, r) space, which corresponds to several aspects such as membership degree, non-membership degree, and reliability component, respectively. In the view of this three-dimensional space, the expert nodes $Q_i(a_i, b_i, c_i)$ are distributed in the C-IF domain. And these expert nodes will be drawn towards the central equilibrium point $Q^{*}(a^{*}, b^{*}, c^{*})$ together, which indicates the situation related to the perspective of cosmic expansion in the formation of consensus.

Together, the two visualizations connect the intuitive and geometric understanding of the OCP. The 2D light-source model emphasizes the direction and intensity of expert attraction, while the 3D spatial model captures the complete convergence behavior in the (μ, ν, r) domain, providing a vivid conceptual foundation for the subsequent construction of the aggregated collective matrix.

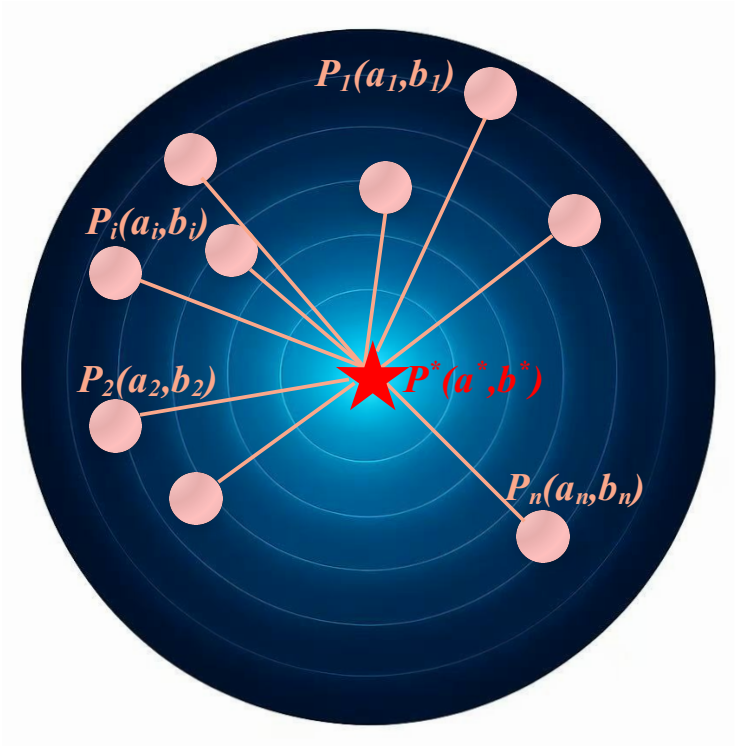


Figure 1. Two-dimensional geometric illustration of the Optimal Consensus Point (OCP).

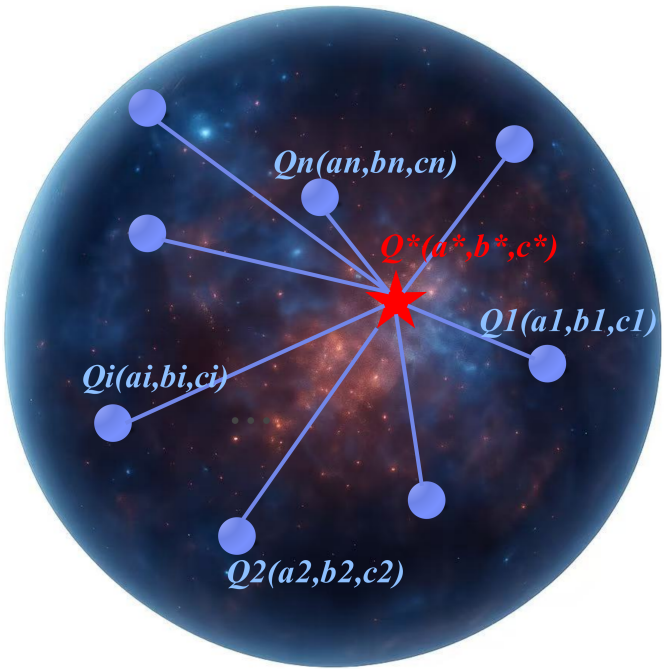


Figure 2. Three-dimensional representation of the OCP in (μ, ν, r) space.

4.3. Notation, Feasible Set, and Problem Statement

Let K experts $(k = 1, \ldots, K)$ evaluate alternative z_i on attribute a_j using C-IFNs, where γ_k denotes the normalized credibility (weight) of expert k:

$$P_{ij} = \{p_{ijk} = (\mu_{ijk}, \nu_{ijk}, r_{ijk}) \in \Omega \mid k = 1, \ldots, K\}, \qquad \sum_{k=1}^{K} \gamma_k = 1,\ \gamma_k \geq 0. \tag{18}$$

The constraint $\gamma_k \geq 0$ ensures that each expert contributes non-negatively to the aggregation process, while the normalization condition $\sum_{k=1}^{K} \gamma_k = 1$ interprets $\{\gamma_k\}$ as a

convex weighting scheme. This normalization is not intended to restrict individual γ_k to be less than one in isolation, but to guarantee scale invariance of the objective function and to prevent any single expert from dominating the aggregation due to magnitude effects. Such normalized credibility weights are standard in weighted consensus and aggregation models.

The feasible domain introduced in Section 3 is

$$\Omega = \{(\mu, \nu, r) : \ \mu \geq 0, \ \nu \geq 0, \ \mu^2 + \nu^2 \leq 1, \ 0 \leq r \leq 1\}. \tag{19}$$

Explanation. Ω is convex (unit disk in (μ, ν) with nonnegativity, and a segment for r), so feasibility projection is well-posed. The aggregation problem is to determine $x_{ij}^* \in \Omega$ minimizing $f_{ij}(x)$ for each cell and then assemble all x_{ij}^* into a consensus matrix.

4.3.1. Cell-Wise Objective and Global Separability

$$x_{ij}^* = \arg\min_{x \in \Omega} f_{ij}(x) = \arg\min_{x \in \Omega} \sum_{k=1}^{K} \gamma_k \| W_j (x - p_{ijk}) \|_2 \tag{20}$$

and the global energy $E(x) = \sum_{i=1}^{n} \sum_{j=1}^{m} f_{ij}(x_{ij})$ is separable.

Explanation. Here, separability means that the global optimization problem can be decomposed into independent cell-wise subproblems. This property holds because each objective function $f_{ij}(x_{ij})$ depends only on the local decision variable x_{ij} and does not involve cross-cell coupling terms or shared constraints across different (i, j) pairs. As a result, each cell-wise optimization can be solved independently and in parallel, which is consistent with the proposed algorithmic implementation and significantly reduces computational coupling across attributes and alternatives.

4.3.2. Existence, Convexity, and (Near-)Uniqueness

Because Ω is compact and f_{ij} is continuous and convex (as a finite weighted sum of Euclidean norms composed with a linear map W_j), an optimal solution exists. Moreover, the solution is unique in generic (non-degenerate) configurations, while non-uniqueness may arise only in symmetric or degenerate cases, such as when expert points are collinear or coincide. In such degenerate cases, the set of optimal solutions forms a convex subset of Ω (e.g., a line segment or a face), rather than a single point; any element of this set yields the same objective value and is therefore equally valid for aggregation and subsequent scoring.

Remark. This places our problem in the same class as the weighted Euclidean *Weber problem* (geometric median) but constrained to Ω; CRA acts as a constrained, projection-based solver for this convex objective.

4.3.3. Subgradient and KKT Characterization

The objective function $f_{ij}(x)$ is convex but generally non-differentiable at points where $x = p_{ijk}$ for some k, due to the presence of Euclidean norms. Therefore, optimality is characterized using subgradient analysis.

When $x \neq p_{ijk}$ for all k, the subgradient of f_{ij} is single-valued and given by

$$\partial f_{ij}(x) = \left\{ \sum_{k=1}^{K} \gamma_k \frac{W_j^\top W_j (x - p_{ijk})}{\| W_j (x - p_{ijk}) \|_2} \right\}, \qquad (x \neq p_{ijk} \ \forall k). \tag{21}$$

Since the optimization is performed over the compact feasible set Ω, the first-order optimality condition for the constrained problem can be expressed in terms of the KKT condition. Specifically, an Optimal Consensus Point x_{ij}^* satisfies

$$0 \in \partial f_{ij}(x_{ij}^*) + N_\Omega(x_{ij}^*), \tag{22}$$

where $N_\Omega(x_{ij}^*)$ denotes the normal cone of Ω at x_{ij}^*.

Explanation. Equation (22) states that, at the optimal solution, the weighted attraction directions induced by all expert evaluations are in equilibrium, up to the feasibility forces imposed by the boundary of the circular intuitionistic fuzzy domain Ω. If x_{ij}^* lies in the interior of Ω, the normal cone vanishes and the subgradient balances to zero, indicating perfect geometric equilibrium. If x_{ij}^* lies on the boundary, the normal cone accounts for constraint forces that prevent the solution from leaving Ω. Geometrically, this condition characterizes the OCP as a constrained geometric median of expert evaluations in the C-IF space.

4.4. CRA with Roulette-Based Growth Selection and Deterministic Coordinate Radiation

The proposed CRA follows a single-beam mechanism that integrates *roulette-based growth node selection* with *deterministic coordinate radiation*. At each iteration, a growth node is chosen through the inverse-energy roulette rule, after which a set of axis-aligned candidates in (μ, ν, r) space is generated with a fixed step, projected back to the feasible domain Ω, and the lowest-energy candidate is retained. This procedure can be viewed as a discretized projection–gradient descent process that preserves controlled exploration through stochastic roulette sampling.

Illustration. The overall workflow of CRA is visualized in Figure 3 and consists of three modules arranged in a vertically stacked manner:

- Module I: executes inverse-energy roulette for probabilistic growth node selection;
- Module II: performs deterministic coordinate radiation combined with feasibility projection;
- Module III: checks convergence and updates the working set for the next iteration.

The detailed algorithmic procedures corresponding to the three CRA modules are formally summarized in Algorithm 1, Algorithm 2, and Algorithm 3, respectively.

Together, these modules form the complete iterative loop that drives CRA toward the Optimal Consensus Point.

4.4.1. Initialization

The working set is initialized from the expert points (or their centroid). In our MATLAB implementation, the initial array is directly assigned to the expert set, so each expert evaluation serves as an initial growth node within the feasible domain. This matches the statement `array = A;` in the code.

4.4.2. Growth Node Selection (Inverse-Energy Roulette)

Select a growth node $x^{(t)}$ via

$$\Pr\left(x_\ell^{(t)}\right) = \frac{1/f_{ij}(x_\ell^{(t)})}{\sum_u 1/f_{ij}(x_u^{(t)})}. \tag{23}$$

The inverse-energy roulette mechanism for growth node selection is formally described in Algorithm 1.

Explanation. Equation (23) defines an inverse-energy roulette rule, where each candidate growth node $x_\ell^{(t)}$ is selected with probability proportional to $1/f_{ij}(x_\ell^{(t)})$. Since $f_{ij}(x)$ measures the aggregated weighted distance to expert evaluations, lower values indicate better local consensus quality. The normalization in the denominator ensures $\sum_\ell \Pr(x_\ell^{(t)}) = 1$, so that low-energy nodes are favored while higher-energy nodes still retain a nonzero selection probability, which helps avoid premature concentration on a single basin.

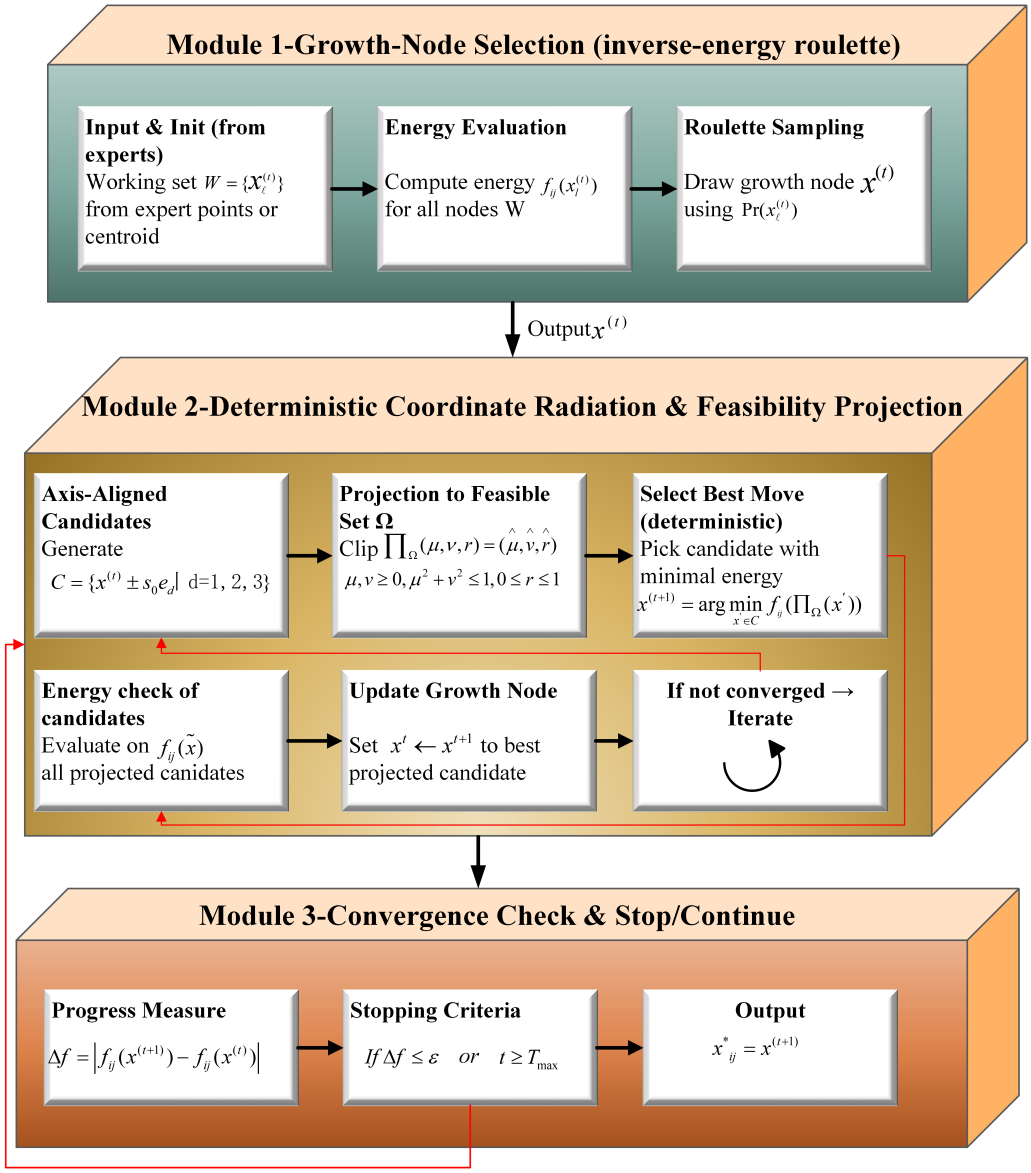


Figure 3. CRA flowchart with three modules: growth node selection, coordinate radiation, and convergence checking. Note. The workflow consists of three vertically stacked modules. Module 1 performs growth node selection via inverse-energy roulette. Module 2 generates and evaluates candidate solutions through deterministic coordinate radiation and feasibility projection. Module 3 checks convergence conditions and determines whether the algorithm stops or continues. Detailed mathematical formulations and parameter definitions are provided in the main text.

4.4.3. Visualization of the Roulette Mechanism

The inverse-energy roulette allocates a higher selection probability to lower-energy nodes, helping the CRA explore multiple regions before convergence.

Explanation. Figure 4 shows how a random number δ determines the selected growth node. This controlled randomness improves early exploration while maintaining overall determinism once the seed is fixed.

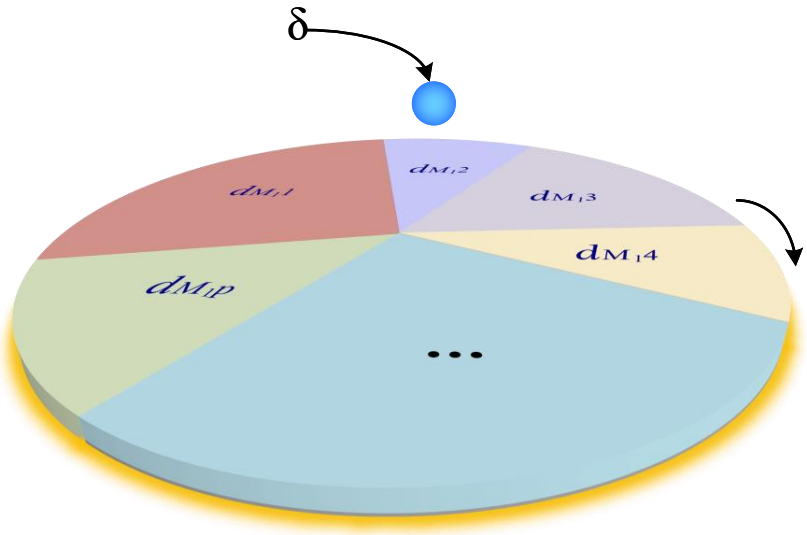


Figure 4. Roulette-based growth node selection mechanism in the CRA algorithm.

Pseudocode (Module I: Growth node selection).

Algorithm 1: CRA Module I: Growth node selection

Input : Working set $\{x_\ell^{(t)}\}$; objective $f_{ij}(\cdot)$; numerical floor eps; random seed (optional)

Output: Growth node $x^{(t)}$

for *each* $x_\ell^{(t)}$ *in working set* **do**

  $f_\ell \leftarrow f_{ij}(x_\ell^{(t)})$

$p_\ell \leftarrow \dfrac{1/\max(\text{eps}, f_\ell)}{\sum_u 1/\max(\text{eps}, f_u)}$

Sample index m according to $\{p_\ell\}$

return $x^{(t)} \leftarrow x_m^{(t)}$

4.4.4. Coordinate Radiation and Feasibility Projection

Form coordinate candidates with fixed step s_0:

$$\mathcal{C} = \{\, x^{(t)} \pm s_0 e_d \mid d = 1,2,3 \,\}, \qquad e_d \text{ are the coordinate basis vectors.} \tag{24}$$

To ensure that each candidate remains a valid circular intuitionistic fuzzy number, a feasibility projection operator Π_Ω is applied:

$$\Pi_\Omega(\mu, \nu, r) = (\hat{\mu}, \hat{\nu}, \hat{r}), \qquad \hat{r} = \min(1, \max(0, r)). \tag{25}$$

The projection of the (μ, ν) components is defined as

$$(\bar{\mu}, \bar{\nu}) = \big(\max(0, \mu),\, \max(0, \nu)\big), \qquad (\hat{\mu}, \hat{\nu}) = \begin{cases} (\bar{\mu}, \bar{\nu}), & \bar{\mu}^2 + \bar{\nu}^2 \le 1, \\ \dfrac{(\bar{\mu}, \bar{\nu})}{\sqrt{\bar{\mu}^2 + \bar{\nu}^2}}, & \text{otherwise.} \end{cases} \tag{26}$$

Explanation. Equation (26) implements the feasibility projection for the CIFN domain $\Omega = \{(\mu, \nu) \mid \mu \geq 0,\ \nu \geq 0,\ \mu^2 + \nu^2 \leq 1\}$. First, $(\bar{\mu}, \bar{\nu})$ enforces the nonnegativity constraints by component-wise truncation. If the resulting point already lies inside the unit quarter-disk, it is kept unchanged; otherwise, it is radially projected onto the boundary $\mu^2 + \nu^2 = 1$ by normalization. Together with the clipping of r in Equation (25), this guarantees that $\Pi_\Omega(\mu, \nu, r) \in \Omega$ always holds, so that every candidate remains a valid circular intuitionistic fuzzy number.

Choose the best projected candidate:

$$x^{(t+1)} = \arg\min_{x' \in \mathcal{C}} f_{ij}\big(\Pi_\Omega(x')\big). \tag{27}$$

The complete coordinate radiation and feasibility projection procedure is summarized in Algorithm 2.

Explanation. The update rule in Equation (27) corresponds to a deterministic coordinate radiation step, where feasibility is enforced through Π_Ω. This design preserves the circular coupling between μ and ν while ensuring that the search remains within the admissible CIFN domain.

Pseudocode (Module II: Coordinate radiation and feasibility projection).

Algorithm 2: CRA Module II: Coordinate radiation and feasibility projection

Input : $x^{(t)}$; fixed step s_0; projection $\Pi_\Omega(\cdot)$; objective $f_{ij}(\cdot)$
Output: $x^{(t+1)}$

Form candidate set:
  $\mathcal{C} = \{\, x^{(t)} + s_0 e_d,\ x^{(t)} - s_0 e_d \mid d = 1, 2, 3 \,\}$
for *each* $x' \in \mathcal{C}$ **do**
  $\tilde{x} \leftarrow \Pi_\Omega(x')$
  $g(\tilde{x}) \leftarrow f_{ij}(\tilde{x})$
$x^{(t+1)} \leftarrow \arg\min_{\tilde{x}} g(\tilde{x})$
return $x^{(t+1)}$

4.4.5. Termination, Parameters, and Numerical Safeguards

The convergence checking and update strategy of CRA is detailed in Algorithm 3.

Use a fixed step $s_t = s_0$ and stop if

$$|f_{ij}(x^{(t+1)}) - f_{ij}(x^{(t)})| < \varepsilon \quad \text{or} \quad t \geq T_{\max}. \tag{28}$$

Implementation note. The MATLAB R2023a implementation uses the iteration cap $T_{\max}$ as the sole stopping rule; the tolerance ε is kept in the theoretical formulation and can be enabled without changing the algorithmic flow.

Default parameters follow the implementation:

$$T_{\max} = 100{,}000,\ s_0 = 10^{-4},\ \gamma = [0.3146,\ 0.3165,\ 0.3689],\ \sum_k \gamma_k = 1. \tag{29}$$

Distances are clipped by $\max(\cdot, \text{eps})$ to avoid division by zero in inverse-energy sampling and to stabilize candidate comparisons.

Pseudocode (Module III: Convergence and update).

Algorithm 3: CRA Module III: Convergence and update

Input : $x^{(t)}$, $x^{(t+1)}$; tol. ε; iter. t; cap $T_{\max}$; working set $\mathcal{W}$
Output: Stop/continue; OCP x_{ij}^{*} (if stop)

if $\left|f_{ij}(x^{(t+1)}) - f_{ij}(x^{(t)})\right| < \varepsilon$ ***or*** $t \geq T_{\max}$ **then**
  return ***Stop*** *and output* $x_{ij}^{*} \leftarrow x^{(t+1)}$
Update working set $\mathcal{W}$ with $x^{(t+1)}$ (consistent with implementation)
return ***Continue***

4.4.6. Computational Complexity and Implementation Mapping

Per iteration, after roulette selection of a growth node, at most six candidates (three axes $\times$ $\pm$) are evaluated. The per-cell objective-evaluation cost is $O(K\,T_{\max})$, and cells are independent and parallelizable. The MATLAB modules map as: `func_distance` $\leftrightarrow$ $f_{ij}(x)$, `func_fitness` $\leftrightarrow$ inverse-energy growth node selection, `func_updated_array` $\leftrightarrow$ coordinate radiation and projection, `func_drawing` $\leftrightarrow$ visualization of convergence.

4.5. Construction of the Aggregated Consensus Matrix

Once each OCP x_{ij}^{*} is obtained, assemble the consensus matrix

$$C = [x_{ij}^{*}], \qquad x_{ij}^{*} = (\mu_{ij}^{*}, \nu_{ij}^{*}, r_{ij}^{*}) \in \Omega. \tag{30}$$

Explanation. Each entry is feasible by projection, preserving the coupling among (μ, ν, r). The matrix C provides a geometrically coherent summary of expert opinions and is compatible with projection-type scoring in C-IF environments [13].

Visualization of the Matrix Construction Process

After the Optimal Consensus Points are obtained, the CRA aggregates them into the final collective matrix.

Explanation. Figure 5 illustrates how the CRA converts geometric consensus points into the collective matrix C, integrating expert preferences across all attributes and alternatives.

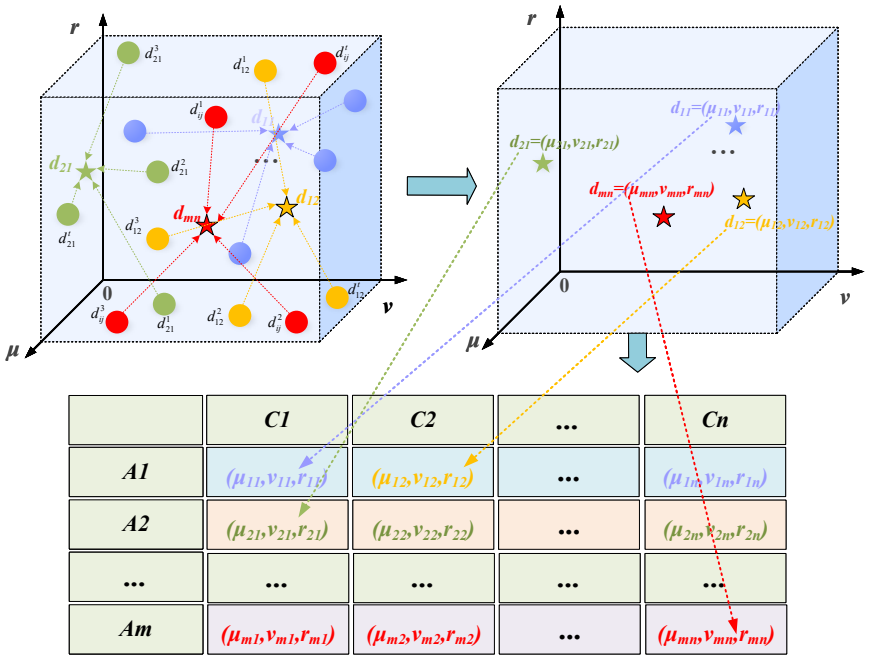


Figure 5. The process of the optimal expert preference collective matrix construction.

4.6. Projection-Based Evaluation and Ranking in (μ, ν, r)

Building on projection-based scoring ideas in neutrosophic settings and extending them to the CIFN embedding used here, we treat μ as benefit-type, while ν (nonmembership) and r (uncertainty radius) are cost-type components. All formulas are expressed directly in (μ, ν, r). Let $\{\omega_j\}$ be nonnegative attribute weights (typically $\sum_j \omega_j = 1$). Note that attribute weights are introduced only in this projection-based scoring stage, while the aggregation stage in Section 4.2 adopts $W_j = I_3$.

Triplet embedding. For each aggregated entry, write $x_{ij}^* = (\mu_{ij}^*, \nu_{ij}^*, r_{ij}^*)$.

Attribute-wise positive/negative ideals. For each attribute j, the extrema used to build the ideal vectors are summarized in Table 1.

Table 1. Attribute-wise extrema for constructing the ideal vectors.

Component	Positive-Side Extremum	Negative-Side Extremum
μ	$\tilde{\mu}_{\max,j} = \max_i \mu_{ij}^*$	$\tilde{\mu}_{\min,j} = \min_i \mu_{ij}^*$
ν	$\tilde{\nu}_{\min,j} = \min_i \nu_{ij}^*$	$\tilde{\nu}_{\max,j} = \max_i \nu_{ij}^*$
r	$\tilde{r}_{\min,j} = \min_i r_{ij}^*$	$\tilde{r}_{\max,j} = \max_i r_{ij}^*$

The ideal vectors are then

$$A^+ = (\tilde{\mu}_{\max}, \tilde{\nu}_{\min}, \tilde{r}_{\min}), \qquad A^- = (\tilde{\mu}_{\min}, \tilde{\nu}_{\max}, \tilde{r}_{\max}). \tag{31}$$

Remark. The subsequent projections are performed on the benefit-mapped triplets $\widehat{\mathbf{x}}_{ij}$ and $\widehat{\mathbf{a}}_j^{\pm}$ defined in (32).

Benefit-oriented mapping. After this mapping, all three components become benefit-type $(\mu,\ 1-\nu,\ 1-r)$; hence, each projection component enters additively.

Define benefit-mapped vectors by

$$\begin{aligned} \widehat{\mathbf{x}}_{ij} &= (\mu_{ij}^*,\ 1-\nu_{ij}^*,\ 1-r_{ij}^*), \\ \widehat{\mathbf{a}}_j^{+} &= (\tilde{\mu}_{\max,j},\ 1-\tilde{\nu}_{\min,j},\ 1-\tilde{r}_{\min,j}), \\ \widehat{\mathbf{a}}_j^{-} &= (\tilde{\mu}_{\min,j},\ 1-\tilde{\nu}_{\max,j},\ 1-\tilde{r}_{\max,j}). \end{aligned} \tag{32}$$

Projection-based closeness (alternative A_i).

$$\mathrm{Prj}_{A_i}^{+} = \frac{\sum_j \widehat{\mu}_{ij}\,\widehat{\mu}_j^{+}\,\omega_j}{\sqrt{\sum_j (\widehat{\mu}_j^{+})^2\,\omega_j}} + \frac{\sum_j \widehat{\nu}_{ij}\,\widehat{\nu}_j^{+}\,\omega_j}{\sqrt{\sum_j (\widehat{\nu}_j^{+})^2\,\omega_j}} + \frac{\sum_j \widehat{r}_{ij}\,\widehat{r}_j^{+}\,\omega_j}{\sqrt{\sum_j (\widehat{r}_j^{+})^2\,\omega_j}} \tag{33}$$

$$\mathrm{Prj}_{A_i}^{-} = \frac{\sum_j \widehat{\mu}_{ij}\,\widehat{\mu}_j^{-}\,\omega_j}{\sqrt{\sum_j (\widehat{\mu}_j^{-})^2\,\omega_j}} + \frac{\sum_j \widehat{\nu}_{ij}\,\widehat{\nu}_j^{-}\,\omega_j}{\sqrt{\sum_j (\widehat{\nu}_j^{-})^2\,\omega_j}} + \frac{\sum_j \widehat{r}_{ij}\,\widehat{r}_j^{-}\,\omega_j}{\sqrt{\sum_j (\widehat{r}_j^{-})^2\,\omega_j}}. \tag{34}$$

Final score (larger is better).

$$S(A_i) = \mathrm{Prj}_{A_i}^{+} + \mathrm{Prj}_{A_i}^{-}. \tag{35}$$

With alternatives ranked in descending order of $S(A_i)$.

Explanation. The (μ, ν, r) embedding isolates the roles of support, hesitation, and opposition; the projection terms implement geometric similarity to ideal points and are consistent with modern information-measure-based scoring mechanisms employed in probabilistic linguistic and C-IF consensus models [17,40].

4.7. Quality Assessment and Sensitivity

We evaluate fidelity and robustness using four indicators computed from C and $\{E_k\}$. For reference, the average information energy of expert matrices $IE(E)$ is also reported to compare the concentration before and after aggregation.

4.7.1. Hamming Distance (Dispersion)

$$H(C,E_k)=\frac{1}{3mn}\sum_{i=1}^{n}\sum_{j=1}^{m}\Big(|\mu_{ij}^{*}-\mu_{ijk}|+|\nu_{ij}^{*}-\nu_{ijk}|+|r_{ij}^{*}-r_{ijk}|\Big),\qquad \overline{H}=\frac{1}{K}\sum_{k}H(C,E_k). \tag{36}$$

4.7.2. Similarity (Coherence)

$$S(C,E_k)=1-H(C,E_k),\qquad \overline{S}=1-\overline{H}. \tag{37}$$

4.7.3. Correlation (Structural Alignment)

Flatten (μ,ν,r) into vectors and compute

$$K(C,E_k)=\frac{\sum_u(x_u^C-\bar{x}^C)(x_u^k-\bar{x}^k)}{\sqrt{\sum_u(x_u^C-\bar{x}^C)^2}\sqrt{\sum_u(x_u^k-\bar{x}^k)^2}},\qquad \overline{K}=\frac{1}{K}\sum_{k}K(C,E_k). \tag{38}$$

4.7.4. Information Energy (Compactness)

$$E(C)=\frac{1}{mn}\sum_{i=1}^{n}\sum_{j=1}^{m}\left[(\mu_{ij}^{*})^2+(\nu_{ij}^{*})^2+(r_{ij}^{*})^2\right]. \tag{39}$$

5. Results and Comparative Analysis

5.1. Dataset Description and Source

To verify the validity of the proposed CRA-based aggregation model, we adopt the same practical group decision-making problem discussed in Li et al. [41] and Xu [42], which was later used as a benchmark case in Khan et al. [17]. This benchmark evaluates seven agroecological zones in Hubei Province, China.

Hubei Province is located in Central China along the middle reaches of the Yangtze River and is known for cultivating diverse crops. However, the agricultural development in this region is actually constrained in many aspects. For instance, land resources are limited and cannot be utilized without limit. The environment is continuously deteriorating, which is very unfavorable for agricultural production. The population pressure is also constantly increasing, which adds many obstacles to agricultural development. To mitigate these challenges, Hubei Province was divided into seven distinct agroecological zones based on environmental and resource characteristics: Wuhan–Ezhou–Huanggang (z_1), Northeast Hubei (z_2), Southeast Hubei (z_3), Jianghan region (z_4), North Hubei (z_5), Northwest Hubei (z_6), and Southwest Hubei (z_7).

A committee of three decision-makers was constituted to rank these seven regions according to their overall agroecological performance. Each expert provided pairwise comparisons between every two zones, expressed as C-IFPRs, where each element $a_{ij}=(\mu_{ij},\nu_{ij};r_{ij})$ represents preference, non-preference, and radius uncertainty. The membership and non-membership values follow the original data of Xu [42], while the radius component r_{ij} was introduced in Khan et al. [17] to extend the intuitionistic fuzzy representation into circular form. Hence, each expert's evaluation is a 7×7 C-IFPR matrix $A_\ell=(\mu_{ij}^{\ell},\nu_{ij}^{\ell};r_{ij}^{\ell})$ for $\ell=1,2,3$; the three matrices are reported in Tables 2–4. For readability

(and following Khan et al. [17]), each A_ℓ is displayed in two blocks (rows/columns Z_1–Z_4 and Z_5–Z_7).

Note. All computations in this section follow the CRA framework and equations in Section 4, especially Equations (16)–(39).

Table 2. C-IFPR matrix of Expert 1, A_1.

	z_1	z_2	z_3	z_4
z_1	(0.50, 0.50; 0.00)	(0.50, 0.20; 0.07)	(0.70, 0.10; 0.07)	(0.50, 0.30; 0.07)
z_2	(0.20, 0.50; 0.06)	(0.50, 0.50; 0.00)	(0.60, 0.20; 0.06)	(0.30, 0.60; 0.06)
z_3	(0.10, 0.70; 0.05)	(0.20, 0.60; 0.05)	(0.50, 0.50; 0.00)	(0.30, 0.60; 0.05)
z_4	(0.30, 0.50; 0.08)	(0.60, 0.30; 0.08)	(0.60, 0.30; 0.08)	(0.50, 0.50; 0.00)
z_5	(0.40, 0.60; 0.09)	(0.10, 0.70; 0.09)	(0.50, 0.40; 0.09)	(0.10, 0.60; 0.09)
z_6	(0.10, 0.90; 0.10)	(0.20, 0.80; 0.10)	(0.10, 0.70; 0.10)	(0.10, 0.80; 0.10)
z_7	(0.10, 0.80; 0.01)	(0.30, 0.60; 0.01)	(0.20, 0.70; 0.01)	(0.30, 0.70; 0.01)
	z_5	z_6	z_7	
z_1	(0.60, 0.40; 0.07)	(0.90, 0.10; 0.07)	(0.80, 0.10; 0.07)	
z_2	(0.70, 0.10; 0.06)	(0.80, 0.20; 0.06)	(0.60, 0.30; 0.06)	
z_3	(0.40, 0.50; 0.05)	(0.70, 0.10; 0.05)	(0.70, 0.20; 0.05)	
z_4	(0.60, 0.10; 0.08)	(0.80, 0.10; 0.08)	(0.70, 0.30; 0.08)	
z_5	(0.50, 0.50; 0.00)	(0.50, 0.20; 0.09)	(0.40, 0.10; 0.09)	
z_6	(0.20, 0.50; 0.10)	(0.50, 0.50; 0.00)	(0.30, 0.70; 0.10)	
z_7	(0.10, 0.40; 0.01)	(0.70, 0.30; 0.01)	(0.50, 0.50; 0.00)	

Table 3. C-IFPR matrix of Expert 2, A_2.

	z_1	z_2	z_3	z_4
z_1	(0.50, 0.50; 0.00)	(0.60, 0.10; 0.08)	(0.80, 0.20; 0.08)	(0.60, 0.30; 0.08)
z_2	(0.10, 0.60; 0.04)	(0.50, 0.50; 0.00)	(0.50, 0.10; 0.04)	(0.30, 0.70; 0.04)
z_3	(0.20, 0.80; 0.02)	(0.10, 0.50; 0.02)	(0.50, 0.50; 0.00)	(0.40, 0.60; 0.02)
z_4	(0.30, 0.60; 0.01)	(0.70, 0.30; 0.01)	(0.60, 0.40; 0.01)	(0.50, 0.50; 0.00)
z_5	(0.20, 0.70; 0.09)	(0.10, 0.60; 0.09)	(0.50, 0.30; 0.09)	(0.30, 0.70; 0.09)
z_6	(0.10, 0.80; 0.05)	(0.20, 0.70; 0.05)	(0.20, 0.60; 0.05)	(0.20, 0.80; 0.05)
z_7	(0.20, 0.80; 0.04)	(0.20, 0.60; 0.04)	(0.10, 0.50; 0.04)	(0.20, 0.60; 0.04)
	z_5	z_6	z_7	
z_1	(0.70, 0.20; 0.08)	(0.80, 0.10; 0.08)	(0.80, 0.20; 0.08)	
z_2	(0.60, 0.10; 0.04)	(0.70, 0.20; 0.04)	(0.60, 0.20; 0.04)	
z_3	(0.30, 0.50; 0.02)	(0.60, 0.20; 0.02)	(0.50, 0.10; 0.02)	
z_4	(0.70, 0.30; 0.01)	(0.80, 0.20; 0.01)	(0.60, 0.20; 0.01)	
z_5	(0.50, 0.50; 0.00)	(0.60, 0.20; 0.09)	(0.40, 0.30; 0.09)	
z_6	(0.20, 0.60; 0.05)	(0.50, 0.50; 0.00)	(0.30, 0.60; 0.05)	
z_7	(0.30, 0.40; 0.04)	(0.60, 0.30; 0.04)	(0.50, 0.50; 0.00)	

5.2. Experimental Parameters

The CRA algorithm was employed to aggregate the three expert matrices introduced in Section 5.1. All parameter settings strictly follow the MATLAB implementation described in Section 4, ensuring that the experimental results are consistent with the theoretical formulation.

During each iteration, CRA performs a deterministic geometric search within the feasible domain Ω in Equation (19). The candidate point is updated along the coordinate axes with a fixed step size s_0 by evaluating the set in Equation (24), projected with the operator in Equation (25), and the best move is accepted according to Equation (27). The process repeats until the stopping rule in Equation (28) is satisfied or the maximum iteration cap $T_{\max}$ is reached. The key parameters used in the experiments are summarized in Table 5 and correspond to Equation (29).

Table 4. C-IFPR matrix of Expert 3, A_3.

	z_1	z_2	z_3	z_4
z_1	(0.50, 0.50; 0.00)	(0.60, 0.20; 0.09)	(0.80, 0.10; 0.09)	(0.70, 0.20; 0.09)
z_2	(0.20, 0.60; 0.03)	(0.50, 0.50; 0.00)	(0.60, 0.10; 0.03)	(0.20, 0.70; 0.03)
z_3	(0.10, 0.80; 0.04)	(0.10, 0.60; 0.04)	(0.50, 0.50; 0.00)	(0.20, 0.30; 0.04)
z_4	(0.20, 0.70; 0.07)	(0.70, 0.20; 0.07)	(0.30, 0.20; 0.07)	(0.50, 0.50; 0.00)
z_5	(0.20, 0.80; 0.05)	(0.20, 0.60; 0.05)	(0.40, 0.30; 0.05)	(0.20, 0.60; 0.05)
z_6	(0.10, 0.90; 0.09)	(0.10, 0.80; 0.09)	(0.10, 0.90; 0.09)	(0.10, 0.80; 0.09)
z_7	(0.10, 0.70; 0.04)	(0.20, 0.80; 0.04)	(0.10, 0.60; 0.04)	(0.20, 0.70; 0.04)

	z_5	z_6	z_7
z_1	(0.80, 0.20; 0.09)	(0.90, 0.10; 0.09)	(0.70, 0.10; 0.09)
z_2	(0.60, 0.20; 0.03)	(0.80, 0.10; 0.03)	(0.80, 0.20; 0.03)
z_3	(0.30, 0.40; 0.04)	(0.90, 0.10; 0.04)	(0.60, 0.10; 0.04)
z_4	(0.60, 0.20; 0.07)	(0.80, 0.10; 0.07)	(0.70, 0.20; 0.07)
z_5	(0.50, 0.50; 0.00)	(0.70, 0.20; 0.05)	(0.70, 0.30; 0.05)
z_6	(0.20, 0.70; 0.09)	(0.50, 0.50; 0.00)	(0.20, 0.80; 0.09)
z_7	(0.30, 0.70; 0.04)	(0.80, 0.20; 0.04)	(0.50, 0.50; 0.00)

Table 5. Parameter settings of the CRA algorithm.

Symbol	Description	Value
s_0	Step size	10^{-4}
$T_{\max}$	Maximum iteration count	10,000
γ	Expert weights	{0.3146, 0.3165, 0.3689}

Software. The CRA aggregation procedure is implemented in MATLAB. All comparative computations—including projection scoring and the four evaluation indicators (Hamming distance, similarity, correlation coefficient, and information energy)—as well as figures are implemented in Python 3.10.9 (NumPy/Matplotlib). All formulas are exactly those defined in Section 4, in particular Equations (32)–(35) and Equations (36)–(39); no additional normalization or preprocessing was introduced. The only source of randomness is the roulette sampling in Equation (23); fixing the random seed ensures strict reproducibility.

Weights. Expert weights γ follow the same configuration as the C-IFPRs benchmark, as listed in Table 5. Equal attribute weights ($\omega_j = 1/7$) are used to ensure that performance differences stem solely from the aggregation mechanism.

5.3. Aggregation Results of Two Methods

5.3.1. C-IFPRs Aggregated Matrix

The collective matrix obtained by the C-IFPRs method $\widehat{A}^{\mathrm{C-IFPRs}}$ (four-decimal format) is provided in Table 6. Each entry follows the notation $(\mu, \nu; r)$, where μ and ν denote the membership and non-membership degrees, respectively, and r is the circular uncertainty radius.

5.3.2. CRA-Aggregated Matrix

Table 7 presents the collective matrix $\widehat{A}^{\mathrm{CRA}}$ obtained using the CRA algorithm under identical decision conditions.

Table 6. C-IFPRs aggregated matrix $\widehat{A}^{\mathrm{C-IFPRs}}$.

	z_1	z_2	z_3	z_4
z_1	(0.5000, 0.5000; 0.0000)	(0.6000, 0.2400; 0.0800)	(0.7600, 0.1800; 0.0800)	(0.5900, 0.3000; 0.0800)
z_2	(0.2500, 0.5900; 0.0400)	(0.5000, 0.5000; 0.0000)	(0.5800, 0.2400; 0.0800)	(0.3200, 0.6000; 0.0800)
z_3	(0.1800, 0.7600; 0.0400)	(0.2400, 0.5800; 0.0400)	(0.5000, 0.5000; 0.0000)	(0.5000, 0.3000; 0.0800)
z_4	(0.3000, 0.5900; 0.0500)	(0.6000, 0.3200; 0.0500)	(0.5500, 0.3000; 0.0500)	(0.5000, 0.5000; 0.0000)
z_5	(0.2400, 0.7100; 0.0800)	(0.2300, 0.6100; 0.0800)	(0.4600, 0.3900; 0.0800)	(0.2600, 0.2500; 0.0800)
z_6	(0.0600, 0.8900; 0.0800)	(0.1500, 0.7700; 0.0800)	(0.1800, 0.7300; 0.0800)	(0.1300, 0.8200; 0.0800)
z_7	(0.1100, 0.7600; 0.0300)	(0.2300, 0.6600; 0.0300)	(0.2100, 0.5700; 0.0300)	(0.2300, 0.6800; 0.0300)

	z_5	z_6	z_7
z_1	(0.7100, 0.2300; 0.0800)	(0.8900, 0.0600; 0.0800)	(0.7600, 0.1100; 0.0800)
z_2	(0.6100, 0.2200; 0.0800)	(0.7700, 0.1500; 0.0800)	(0.6600, 0.2300; 0.0800)
z_3	(0.3900, 0.4600; 0.0800)	(0.7300, 0.1700; 0.0800)	(0.5700, 0.2100; 0.0800)
z_4	(0.6400, 0.2500; 0.0500)	(0.8200, 0.1300; 0.0500)	(0.6800, 0.2200; 0.0500)
z_5	(0.5000, 0.5000; 0.0000)	(0.6500, 0.2400; 0.0800)	(0.5400, 0.2900; 0.0800)
z_6	(0.2400, 0.6500; 0.0800)	(0.5000, 0.5000; 0.0000)	(0.3000, 0.6500; 0.0800)
z_7	(0.2900, 0.5400; 0.0300)	(0.0800, 0.3000; 0.0300)	(0.5000, 0.5000; 0.0000)

Table 7. CRA-aggregated matrix $\widehat{A}^{\mathrm{CRA}}$.

	z_1	z_2	z_3	z_4
z_1	(0.5000, 0.5000; 0.0000)	(0.5855, 0.1851; 0.0856)	(0.7855, 0.1149; 0.0856)	(0.6000, 0.3000; 0.0800)
z_2	(0.1846, 0.5854; 0.0359)	(0.5000, 0.5000; 0.0000)	(0.5846, 0.1146; 0.0359)	(0.2729, 0.6794; 0.0414)
z_3	(0.1132, 0.7867; 0.0387)	(0.1133, 0.5868; 0.0387)	(0.5000, 0.5000; 0.0000)	(0.3139, 0.5767; 0.0427)
z_4	(0.2860, 0.5993; 0.0287)	(0.6747, 0.2627; 0.0501)	(0.5706, 0.3137; 0.0626)	(0.5000, 0.5000; 0.0000)
z_5	(0.2118, 0.7096; 0.0838)	(0.1261, 0.6223; 0.0796)	(0.4739, 0.3223; 0.0796)	(0.2000, 0.6000; 0.0500)
z_6	(0.1000, 0.9000; 0.0900)	(0.1688, 0.7792; 0.0865)	(0.1000, 0.7000; 0.1000)	(0.1000, 0.8000; 0.0900)
z_7	(0.1231, 0.7698; 0.0260)	(0.2303, 0.6336; 0.0309)	(0.1000, 0.6000; 0.0400)	(0.2136, 0.6856; 0.0359)

	z_5	z_6	z_7
z_1	(0.7083, 0.2093; 0.0808)	(0.8952, 0.1000; 0.0830)	(0.7720, 0.1221; 0.0778)
z_2	(0.6206, 0.1271; 0.0414)	(0.7770, 0.1711; 0.0467)	(0.6326, 0.2302; 0.0444)
z_3	(0.3220, 0.4703; 0.0325)	(0.7000, 0.1000; 0.0500)	(0.6000, 0.1000; 0.0400)
z_4	(0.6000, 0.2000; 0.0700)	(0.8000, 0.1000; 0.0700)	(0.6889, 0.2131; 0.0646)
z_5	(0.5000, 0.5000; 0.0000)	(0.6000, 0.2000; 0.0900)	(0.4610, 0.2459; 0.0819)
z_6	(0.2000, 0.6000; 0.0500)	(0.5000, 0.5000; 0.0000)	(0.3000, 0.7000; 0.1000)
z_7	(0.2464, 0.4620; 0.0320)	(0.7000, 0.3000; 0.0100)	(0.5000, 0.5000; 0.0000)

5.3.3. Comparative Discussion

labelsubsubsec:agg-comparison As shown in Tables 6 and 7, the overall structural pattern of both matrices is consistent, confirming that the CRA algorithm maintains the transitivity and diagonal neutrality conditions of the original C-IFPRs framework. However, the CRA aggregation produces slightly smaller or comparable uncertainty radii r across most entries (e.g., z_2–z_3, z_5–z_6), while membership values μ display smoother gradation among adjacent alternatives. This indicates a more geometrically balanced consensus state achieved through CRA's radiation–convergence mechanism. The quantitative differences will be further examined in Section 5.4 through projection scoring and the four evaluation indicators.

5.4. Projection Scoring Results Based on the (μ, ν, r) Scheme

Following the projection scoring system defined in Section 4 (see the benefit mapping in Equation (32), the ideal construction in Equation (31), and the projection formulas in Equations (33)–(35)), and using equal attribute weights, we evaluate the alternatives on the two collective matrices in Tables 6 and 7.

5.4.1. Step 1: Ideal Vectors and Denominators

Each aggregated entry is transformed by the benefit-oriented mapping in Equation (32), $\widehat{\mathbf{x}}_{ij} = (\mu_{ij}, 1-\nu_{ij}, 1-r_{ij})$. The positive/negative ideal vectors $\widehat{\mathbf{a}}_j^{+}$ and $\widehat{\mathbf{a}}_j^{-}$ are constructed via Equation (31); the corresponding weighted denominators are those appearing in the projection formulas Equations (33) and (34). Intermediate ideal vectors and denominators are omitted for brevity and reproducibility.

5.4.2. Step 2: Positive/Negative Projections and Scores

According to Equations (33)–(35), we obtain the projections Prj^{+}, Prj^{-} and the final score $S = \mathrm{Prj}^{+} + \mathrm{Prj}^{-}$ (four decimals).

Note that the obtained projection scores $S(A_i)$ are not constrained to $[-1, 1]$, as the CIFN embedding preserves geometric magnitudes of $(\mu, 1-\nu, 1-r)$. For visualization purposes, normalized scores S_{norm01} in $[0, 1]$ are additionally reported in Tables 8 and 9, which do not affect the ranking.

Table 8. C-IFPRs: projections and scores ((μ, ν, r) projection, normalized to [0,1]).

Alt	$\mathbf{Prj}^{+}$	$\mathbf{Prj}^{-}$	S	$S_{\mathbf{norm01}}$	Rank
z_1	2.3838	2.3450	4.7288	1.0000	1
z_2	2.1356	2.0966	4.2322	0.7259	3
z_3	1.9499	1.8996	3.8495	0.5147	4
z_4	2.2280	2.1888	4.4169	0.8273	2
z_5	1.9298	1.9131	3.8429	0.5110	5
z_6	1.4806	1.4364	2.9170	0.0000	7
z_7	1.6556	1.6795	3.3351	0.2308	6

Table 9. CRA: projections and scores ((μ, ν, r) projection, normalized to [0,1]).

Alt	$\mathbf{Prj}^{+}$	$\mathbf{Prj}^{-}$	S	$S_{\mathbf{norm01}}$	Rank
z_1	2.3912	2.3466	4.7378	1.0000	1
z_2	2.1717	2.1428	4.3144	0.7643	3
z_3	1.9537	1.9494	3.9031	0.5353	4
z_4	2.2435	2.1991	4.4426	0.8357	2
z_5	1.8758	1.8664	3.7422	0.4458	5
z_6	1.4643	1.4770	2.9414	0.0000	7
z_7	1.7530	1.7835	3.5365	0.3313	6

Rankings.

C-IFPRs: $z_1 \succ z_4 \succ z_2 \succ z_3 \succ z_5 \succ z_7 \succ z_6$.

CRA: $z_1 \succ z_4 \succ z_2 \succ z_3 \succ z_5 \succ z_7 \succ z_6$.

Discussion. Although the proposed CRA method and the benchmark C-IFPR-based approaches produce the same ranking order in this illustrative example, this consistency should be interpreted as a desirable property rather than a limitation. It indicates that CRA is compatible with existing methods under relatively regular and well-structured preference information. However, the key advantage of CRA lies not in altering rankings for such ideal cases, but in its geometric aggregation mechanism. Specifically, CRA operates directly on the embedded CIFN representations of expert opinions, preserving geometric magnitudes and uncertainty radii, and determines the final decision via energy minimization toward an Optimal Consensus Point. This design avoids reliance on predefined aggregation operators or consistency-repair procedures, and provides improved robustness and interpretability in scenarios with heterogeneous, conflicting, or noisy expert evaluations, as further demonstrated in the subsequent analyses.

5.4.3. Step 3: Four-Indicator Comparison

Using the definitions in Equations (36)–(39), Table 10 reports the quality indicators of the two collective matrices (C-IFPRs = original method, CRA = our method). For interpretation, among the four indicators, Hamming represents dispersion (smaller is better), whereas Cosine, Pearson, and information energy indicate coherence or compactness (larger is better).

Table 10. Quality indicators of the aggregation matrices (four decimals).

Metric	C-IFPRs	CRA
Hamming	0.0322	0.0144
Cosine	0.9832	0.9987
IE(M)	0.1624	0.1640
IE(E)	0.1626	0.1626
Pearson	0.9608	0.9971

It is worth noting that the proposed CRA framework does not involve entropy-based weighting or uncertainty modeling; instead, the information energy (Equation (39)) serves as a deterministic compactness indicator.

5.4.4. Step 4: Visual Comparison

To provide an intuitive comparison, Figures 6 and 7 together illustrate the performance of C-IFPRs and CRA in terms of the final projection scores and the normalized quality indicators.

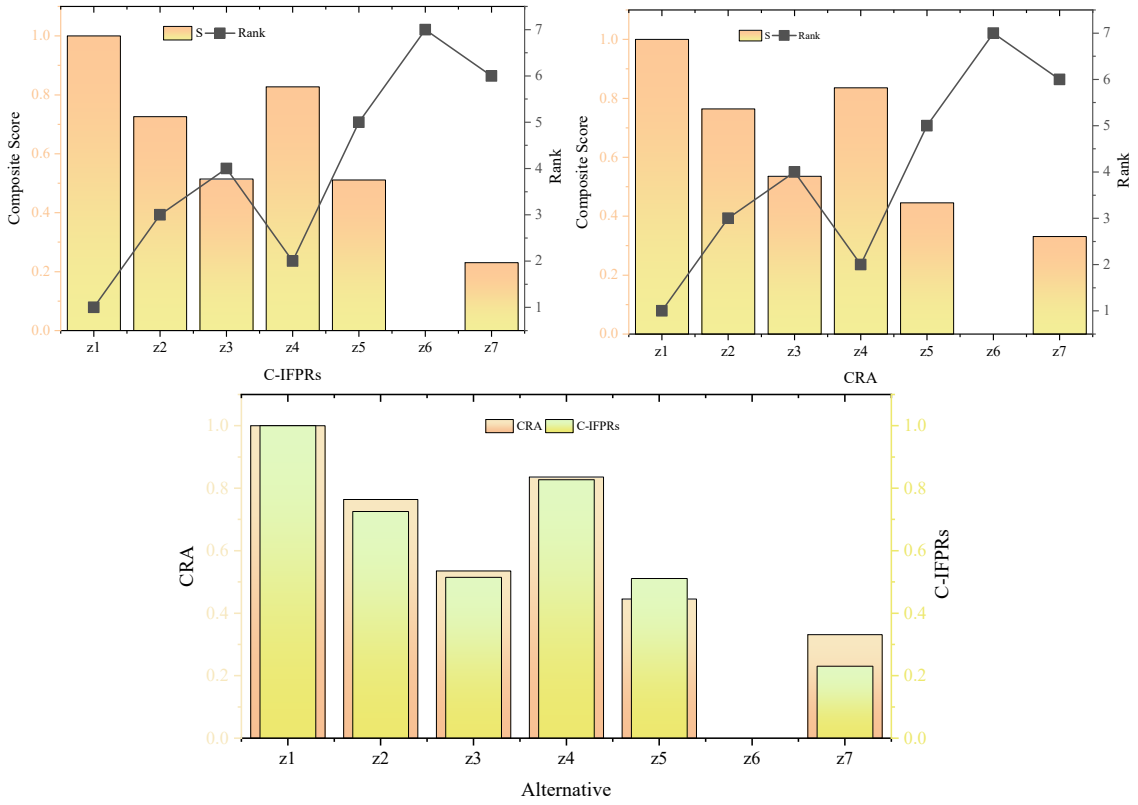


Figure 6. Comparison of composite scores and rankings between C-IFPRs and CRA models.

Description. Figure 6 presents the composite scores (S) and corresponding rankings of the seven alternatives under both aggregation models. The upper panels display the S-rank distributions for C-IFPRs and CRA, while the lower panel compares their normalized scores directly. Both models yield identical ranking patterns across all alternatives, confirming the consistency of the projection-based evaluation. CRA produces slightly higher and more

evenly distributed scores, indicating enhanced numerical stability and stronger consensus concentration compared with the original C-IFPR aggregation.

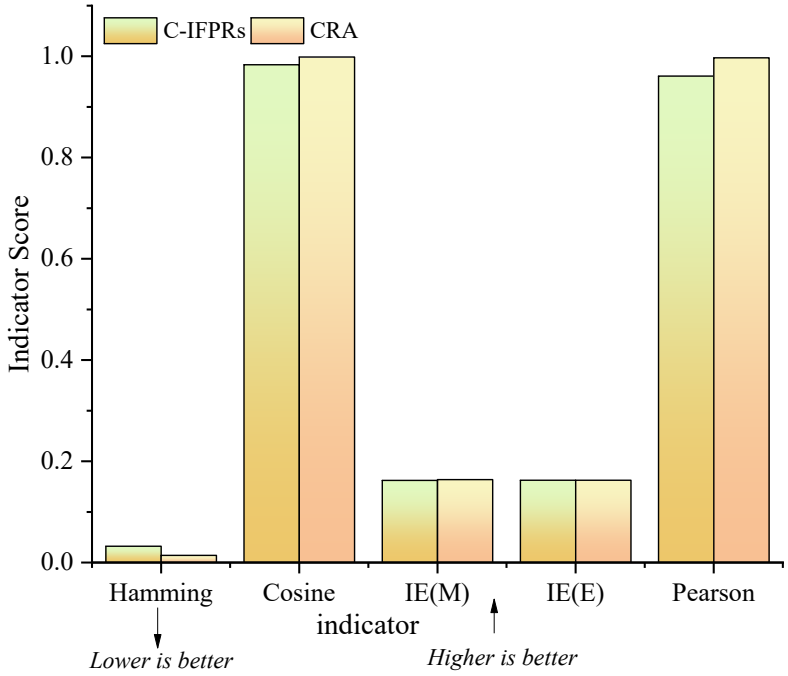


Figure 7. Normalized comparison of evaluation indicators between C-IFPRs and CRA.

Further analysis. Figure 7 visualizes the normalized values of four evaluation indicators. We can clearly observe that CRA has achieved a higher overall performance than before in terms of the Hamming index, the Cosine index, the IE(M) index, the IE(E) index, and the Pearson index. This situation indicates that both aggregation consistency and information compactness have been improved to a certain extent.

5.4.5. Step 5: Ranking and Remarks

The two methods finally produced the same ranking result, which confirmed that the proposed CRA aggregation actually retains the decision consistency of the original C-IFPRs framework. The projected score produced by the CRA model is slightly higher and more stable. This is consistent with the improvement observed in the Hamming, cos, and Pearson indicators. For details, please refer to (Table 10). These findings indicate that within the (μ, ν, r) projection framework mentioned in Section 4, CRA achieved a smoother and more coherent consensus surface while maintaining diagonal neutrality.

The final scores and rankings were conducted in accordance with the projection-based TOPSIS paradigm recently applied in MAGDM research, which can be referred [43]. Based on this, CRA introduces custom adaptations that are consistent with the u–v–r representation defined in the formula. Here, the formula refers to Equations (32)–(35). As can be seen from Table 8 and Table 9 , the sorting order of the results it shows is the same as that in reference [17]. This makes it convenient to directly compare methods among all the aggregation models.

5.5. Parameter Sensitivity Analysis

To evaluate the sensitivity and numerical stability of the CRA algorithm, a series of experiments was conducted by varying its two main control parameters, namely the initial step size s_0 and the maximum number of iterations $T_{\max}$. Different parameter combinations were tested repeatedly on the same dataset to empirically identify configurations that yield stable convergence behavior.

Table 11 lists the parameter settings considered in the sensitivity analysis, together with their expected qualitative behaviors.

Table 11. Parameter configurations considered in the sensitivity analysis.

Case	Step Size s_0	Max Iterations $T_{\max}$	Expected Behavior
Baseline	1.0×10^{-4}	10,000	Balanced and stable convergence
A	1.0×10^{-1}	10,000	Overshooting and oscillation
B	1.0×10^{-2}	10,000	Slightly faster convergence
C	1.0×10^{-3}	10,000	Fast and stable convergence
D	1.0×10^{-4}	100	Early stopping, partial convergence
E	1.0×10^{-4}	1000	Moderate stability

Each configuration was executed on the same three-expert dataset, and the resulting aggregated matrices were evaluated using five quantitative indicators: Hamming distance (dispersion, ↓), Cosine similarity (coherence, ↑), information energy for the aggregated matrix and for experts (IE(M), IE(E), ↑), and Pearson correlation (alignment, ↑). The quantitative evaluation results corresponding to these parameter settings are summarized in Table 12, while Figure 8 provides a visual comparison.

Table 12. Performance comparison under different parameter settings (six-decimal precision).

Case	Hamming↓	Cosine↑	IE(M)↑	IE(E)↑	Pearson↑
Baseline	0.014421	0.998725	0.164014	0.162600	0.997120
A	0.023328	0.997374	0.166683	0.162600	0.994214
B	0.014497	0.998702	0.163884	0.162600	0.997069
C	0.014460	0.998721	0.164008	0.162600	0.997113
D	0.025996	0.996272	0.165246	0.162600	0.991875
E	0.024873	0.996834	0.165952	0.162600	0.992899

Remark on Energy Consistency

The information energy of the expert matrices $IE(E)$ remains constant across all parameter settings, since the original expert opinions are identical and not affected by algorithmic parameters. Only the information energy of the aggregated matrix $IE(M)$ varies with the CRA configuration, reflecting changes in the compactness and coherence of the final consensus structure.

The results indicate that the CRA algorithm exhibits strong robustness with respect to small perturbations of s_0 and $T_{\max}$. Overly large step sizes (Case A) caused oscillations and higher dispersion (Hamming↑), while excessively small steps (Case B) slowed down convergence and reduced overall compactness (IE(M)↓). The new Case C ($s_0 = 10^{-3}$) achieved nearly identical performance to the baseline, confirming that CRA remains numerically stable within this range. Reducing the iteration cap (Case D) led to incomplete convergence, whereas increasing $T_{\max}$ moderately (Case E) yielded only minor improvement at a higher computational cost. Consequently, the baseline configuration ($s_0 = 10^{-4}$, $T_{\max} = 10^4$) is adopted for all subsequent numerical analyses due to its optimal trade-off between accuracy and efficiency.

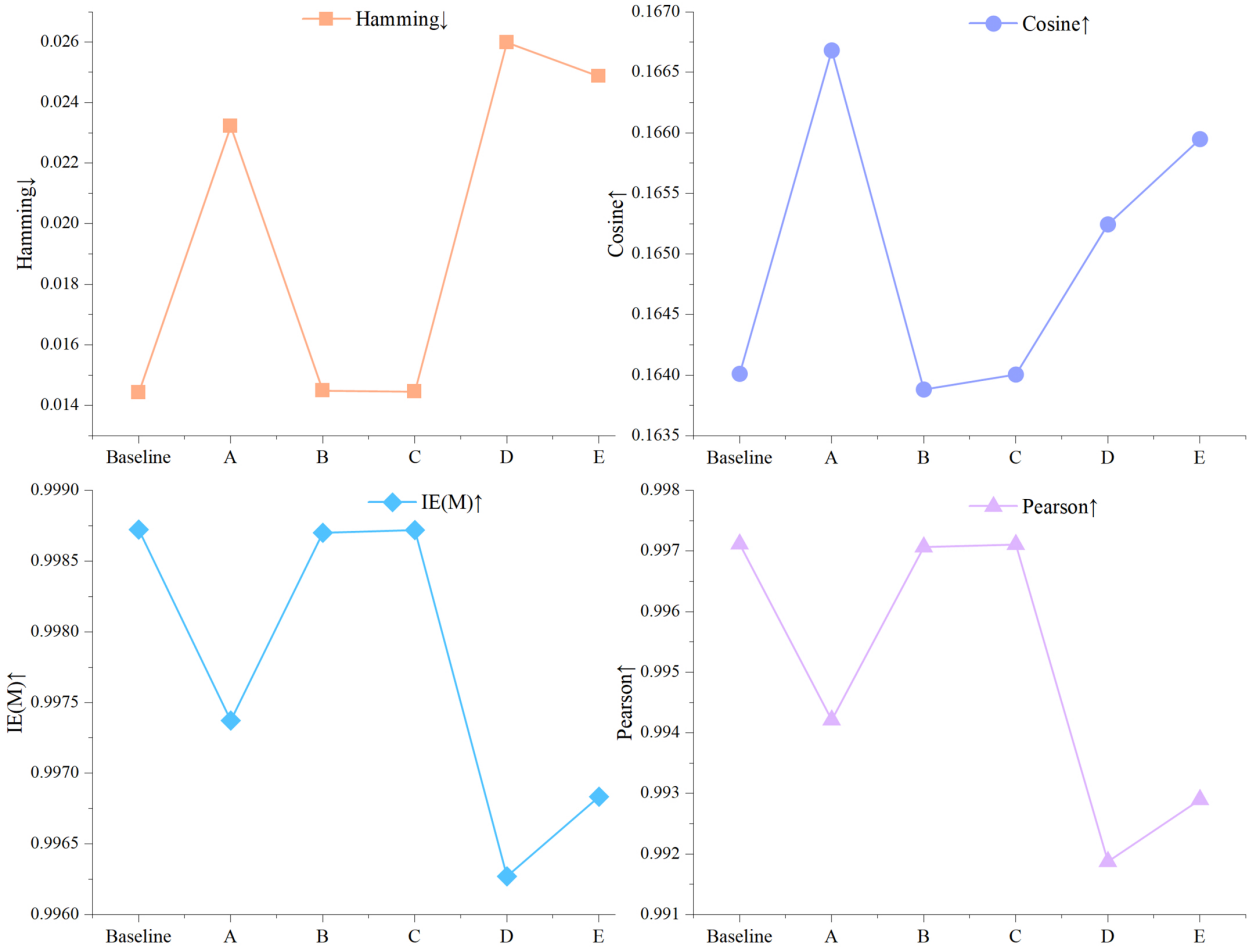


Figure 8. CRA parameter sensitivity analysis across configurations A–E.

5.6. Practical Guidance and Robustness Enhancements

5.6.1. Parameter Guidelines

Based on the sensitivity study in the last section, CRA exhibits a stable convergence region for the step size $s_0 \in [10^{-4}, 10^{-3}]$ with $T_{\max} = 10^4$. In practice, we adopt $s_0 = 10^{-4}$, $T_{\max} = 10^4$ as the default, while $s_0 = 10^{-3}$ offers comparable accuracy with slightly faster convergence. Excessively large steps ($s_0 \approx 10^{-1}$) produce oscillation, and short iteration caps ($T_{\max} \leq 10^3$) lead to incomplete optimization; both settings are therefore discouraged. Increasing $T_{\max}$ beyond 10^4 yields negligible gains on this dataset.

5.6.2. Weights and Usage

Attribute weights $\{\omega_j\}$ are only involved in the projection-based scoring stage (Equations (32)–(35)) and are normalized ($\sum_j \omega_j = 1$). The aggregation stage in Section 4.2 uses $W_j = I_3$. If needed, scalar weighting ($W_j = \sqrt{\omega_j} I_3$) or component-wise diagonal emphasis can be adopted without altering the CRA update rule.

5.6.3. Robustness Remarks

The chosen configuration preserves decision consistency with the C-IFPRs baseline (identical rankings) while maintaining stable convergence across parameter perturbations (Table 12). The CRA framework achieves numerical stability and consensus concentration even under varying step sizes and iteration limits, demonstrating strong robustness in the parameter domain. Regularization on the r-channel to control uncertainty dispersion is a viable extension for future work, but was not activated in our experiments.

5.7. Comparative Analysis with Existing Methods

5.7.1. Step 6: Benchmark Comparison

Following the comparative setting adopted in previous GDM studies [17,42,44–48], we compared the proposed CRA method with seven benchmark algorithms, all applied to the same C-IFPR dataset introduced in Section 5.1. Table 13 reports the alternative rankings of all methods.

Table 13. Comparison of alternative rankings reported by different decision models on the same C-IFPR dataset.

Model	Rankings
IFPR-based model [42]	$z_1 \succ z_4 \succ z_2 \succ z_3 \succ z_5 \succ z_7 \succ z_6$
Dynamic IFPR model [44]	$z_1 \succ z_4 \succ z_2 \succ z_3 \succ z_5 \succ z_7 \succ z_6$
Extended IFPR model [45]	$z_1 \succ z_4 \succ z_2 \succ z_3 \succ z_5 \succ z_7 \succ z_6$
Dynamic preference adjustment model [46]	$z_1 \succ z_4 \succ z_2 \succ z_3 \succ z_5 \succ z_7 \succ z_6$
Consensus-based IFPR model [47]	$z_1 \succ z_4 \succ z_2 \succ z_3 \succ z_5 \succ z_7 \succ z_6$
Distance-driven aggregation model [48]	$z_1 \succ z_4 \succ z_2 \succ z_3 \succ z_5 \succ z_7 \succ z_6$
C-IFPR consensus model [17]	$z_1 \succ z_4 \succ z_2 \succ z_3 \succ z_5 \succ z_7 \succ z_6$
Convergent Radiation Algorithm (CRA)	$z_1 \succ z_4 \succ z_2 \succ z_3 \succ z_5 \succ z_7 \succ z_6$

Methodological clarification. For all benchmark methods listed in Table 13, the alternative rankings were obtained by strictly following the original models and procedures reported in the corresponding references. In particular, the ranking results of the IFPR- and C-IFPR-based benchmark methods are directly adopted from the C-IFPR comparative study [17], where these models were evaluated on the same dataset. The same C-IFPR dataset described in Section 5.1 is therefore used for consistency.

No re-ranking or re-evaluation using the proposed CRA framework was applied to these benchmark methods. The CRA results are produced exclusively by the proposed geometric optimization and projection-based scoring mechanism.

The identical rankings observed in Table 13 indicate that the proposed CRA method is consistent with established IFPR- and C-IFPR-based approaches in classical decision scenarios. However, unlike existing methods that rely primarily on operator-driven aggregation or similarity-based convergence, CRA achieves the same decision outcomes through a fundamentally different geometric optimization mechanism. This consistency under simple scenarios, together with improved robustness and adaptability demonstrated in more complex settings, highlights the methodological advantage of CRA rather than mere ranking differentiation.

5.7.2. Step 7: Overall Assessment

The CRA method preserves the global ranking pattern established by prior approaches (in particular, the best-performing C-IFPR model [17]) and further improves the aggregation quality, as evidenced by the indicator results in Section 5.4 (lower Hamming distance, higher Cosine and Pearson similarity). Compared with entropy-dependent strategies, CRA is parameter-free and geometrically interpretable, offering stronger robustness without sensitivity to entropy definitions.

5.8. Advantages and Limitations of the Study

The proposed CRA-based multi-attribute group decision-making model exhibits several notable advantages over existing aggregation frameworks, particularly when operating under circular intuitionistic fuzzy environments. Nevertheless, certain methodological constraints remain, which could guide future improvements.

5.8.1. Advantages

- Enhanced robustness and geometric interpretability. Unlike entropy-dependent and parameter-tuned algorithms (e.g., [17]), the CRA method operates through a purely geometric optimization process. Without relying on the subjective entropy parameter, it successfully achieved a stable convergence effect and maintained direct interpretability in the (μ, ν) domain. Such attributes enable us to obtain relatively consistent results across different data densities and decision-maker weights.
- After the improvement, both the improved aggregation quality and indicator consistency of the indicators have been enhanced. As shown in Section 5.4, the CRA method outperforms the C-IFPRs method in all four quality indicators. It achieves a lower Hamming distance and also obtains higher cosine correlation and Pearson correlation. The model preserves the overall ranking pattern of benchmark methods (see Table 13) but yields smoother projection distributions and stronger similarity-based coherence among aggregated judgments.

5.8.2. Limitations

- Computational scalability. The iterative geometric search within CRA inevitably increases computational cost as the number of experts or attributes grows. Specifically, for each alternative–attribute cell, CRA performs repeated evaluations of the objective function $f_{ij}(x)$ over multiple candidate points during the radiation–projection–selection cycle. Since the evaluation of $f_{ij}(x)$ involves aggregating distances to all K expert opinions, the per-iteration complexity grows linearly with K. When extended to all alternatives and attributes, the overall runtime may scale approximately quadratically with the problem size in large-scale settings. Nevertheless, the cell-wise separability of the objective function enables efficient parallel implementation, which can significantly mitigate the computational burden in practice.
- Limited generalization to other fuzzy structures. The current model is specifically designed for circular intuitionistic fuzzy numbers (C-IFNs). Although the underlying geometric framework can, in principle, be extended to other fuzzy representations, such as Pythagorean, q-rung orthopair, or interval-valued fuzzy sets, this extension requires additional normalization or embedding mechanisms to ensure boundedness and interpretability in higher-dimensional spaces.

Overall, the CRA model establishes a balanced trade-off between interpretability and accuracy, providing a promising foundation for generalized geometric aggregation in fuzzy group decision-making.

6. Conclusions

This paper proposes a novel Convergent Radiation Algorithm (CRA) for multi-attribute group decision-making (MAGDM) problems in circular intuitionistic fuzzy environments. Starting from the geometric interpretation of circular intuitionistic fuzzy preference relations (C-IFPRs), the CRA framework formulates the aggregation process as a deterministic optimization problem, while ensuring consistency, convergence, and interpretability.

Based on the dataset from the Hubei agro-ecological zone, the empirical results show that, compared with the benchmark C-IFPR model [17], the proposed CRA method achieves higher aggregation quality, smaller internal deviations among experts, and stronger prediction consistency. Furthermore, the comparative analysis presented in Section 5.4 demonstrates that the CRA framework preserves the global ranking order obtained by existing methods, while exhibiting improved robustness in terms of similarity and correlation metrics.

Overall, the CRA framework contributes to the existing literature in three main aspects: (1) it provides a parameter-free geometric mechanism for collective optimization; (2) it offers a stable and interpretable consensus structure without reliance on preprocessing procedures; and (3) it generalizes the classical projection-based decision paradigm to circular intuitionistic fuzzy settings. Future research may extend the CRA framework to hybrid fuzzy environments, investigate its performance on large-scale decision datasets, and incorporate adaptive weighting strategies for dynamic expert reliability evaluation.

Author Contributions: X.L. and J.Q. conceived and designed the study. J.Q. supervised the project and coordinated the overall research activities. Y.G. and T.L. developed the methodology, performed data processing, and implemented the algorithms. X.L. and J.Q. conducted the experiments, analyzed the results, and prepared the tables and figures. Y.G. contributed to the literature review and related work analysis, and assisted in the interpretation of results. J.T., J.Z., and Q.L. provided academic guidance, methodological suggestions, and critical comments that helped improve the quality and clarity of the manuscript. J.Q. and X.L. drafted the main manuscript text. All authors have read and agreed to the published version of the manuscript.

Funding: This study is jointly funded by the National Natural Science Foundation of China (No. 42405175), Natural Science Foundation of Jiangsu Higher Education Institutions of China (No. 24KJB170008), Changzhou Basic Research Program (No. CJ20240030), Changzhou Longcheng Talent Program-Young Scientific and Technological Talent Fostering Project (No. CZTJ-2025-15), and Young Scientific and Technological Talent Fostering Project of Jiangsu Province (No. JSTJ-2025-783).

Data Availability Statement: The data that support the findings of this study are available on request from the corresponding author upon reasonable request.

Conflicts of Interest: The authors declare no conflicts of interest.

List of Abbreviations

MAGDM	Multi-Attribute Group Decision-Making
CIFN	Circular Intuitionistic Fuzzy Number
C-IFPR	Circular Intuitionistic Fuzzy Preference Relation
CRA	Convergent Radiation Algorithm
OCP	Optimal Consensus Point
FPR	Fuzzy Preference Relation
TOPSIS	Technique for Order Preference by Similarity to Ideal Solution

References

1. Zadeh, L.A. Fuzzy sets. *Inf. Control* **1965**, *8*, 338–353. [CrossRef]
2. Chen, T.Y. A circular intuitionistic fuzzy assignment model with a parameterized scoring rule for multiple criteria assessment methodology. *Adv. Eng. Inform.* **2024**, *61*, 102479. [CrossRef]
3. Chen, T.Y. Circular Intuitionistic Fuzzy Median Ranking Model with a Novel Scoring Mechanism for Multiple Criteria Decision Analytics. *Appl. Artif. Intell.* **2024**, *38*, 2335416. [CrossRef]
4. Lei, S.; Ma, X.; Qin, H.; Wang, Y.; Zain, J.M. A new multi-attribute group decision-making method based on Einstein Bonferroni operators under interval-valued Fermatean hesitant fuzzy environment. *Sci. Rep.* **2024**, *14*, 12370. [CrossRef] [PubMed]
5. Sarkar, A.; Görçün, Ö.F.; Ecer, F.; Senapati, T.; Küçükönder, H. Evaluating the financial credibility of third-party logistic providers through a novel Frank operators-driven group decision-making model with dual hesitant linguistic q-rung orthopair fuzzy information. *Eng. Appl. Artif. Intell.* **2025**, *139*, 109483. [CrossRef]
6. Çakır, E.; Taş, M.A. Circular intuitionistic fuzzy decision making and its application. *Expert Syst. Appl.* **2023**, *225*, 120076. [CrossRef]
7. Li, L.; Yang, J. Disturbing fuzzy multi-attribute decision-making method with If weight information is disturbing fuzzy numbers. *Mathematics* **2024**, *12*, 1225. [CrossRef]
8. Chen, T.Y. ORESTE methodology within a circular intuitionistic fuzzy framework for preferential outranking in hybrid cloud service selection. *Appl. Soft Comput.* **2025**, *185*, 113864. [CrossRef]

9. Meher, B.B.; S, J.; Alrasheedi, M. Dombi weighted geometric aggregation operators on the class of trapezoidal-valued intuitionistic fuzzy numbers and their applications to multi-attribute group decision-making. *Artif. Intell. Rev.* **2025**, *58*, 205. [CrossRef]
10. Mishra, A.R.; Chen, S.M.; Rani, P. Multi-attribute decision-making based on picture fuzzy distance measure-based relative closeness coefficients and modified combined compromise solution method. *Inf. Sci.* **2024**, *664*, 120325. [CrossRef]
11. Peng, J.J.; Chen, X.G. A large-scale group decision-making approach based on hesitancy degrees and non-cooperative behaviors with picture fuzzy information. *Appl. Soft Comput.* **2024**, *154*, 111360. [CrossRef]
12. Wang, H. A novel bidirectional projection measures of circular intuitionistic fuzzy sets and its application to multiple attribute group decision-making problems. *AIMS Math.* **2025**, *10*, 10283–10307. [CrossRef]
13. Fahmi, A.; Khan, A.; Maqbool, Z.; Abdeljawad, T. Circular intuitionistic fuzzy Hamacher aggregation operators for multi-attribute decision-making. *Sci. Rep.* **2025**, *15*, 5618. [CrossRef] [PubMed]
14. Khan, S.; Abujabal, H.A.; Rahim, M.; Almutairi, A.; Alburikan, A.; Khalifa, A.E.W. Multi-attribute group decision-making based on quasirung orthopair fuzzy Frank aggregation operators for optimal vehicle selection. *Sci. Rep.* **2025**, *15*, 28868. [CrossRef]
15. Rawat, S.S.; Liu, P.; Stevic, Z.; Senapati, T.; Moslem, S. A novel group decision-making approach based on partitioned Hamy mean operators in q-rung orthopair fuzzy context. *Complex Intell. Syst.* **2024**, *10*, 1375–1408. [CrossRef]
16. Javeed, S.; Javed, M.; Jameel, A.; Senapati, T. A picture fuzzy multi-attribute decision-making approach based on Hamacher Muirhead mean operators. *Granul. Comput.* **2024**, *9*, 64. [CrossRef]
17. Khan, M.J.; Ding, W.; Jiang, S.; Akram, M. Group decision making using circular intuitionistic fuzzy preference relations. *Expert Syst. Appl.* **2025**, *270*, 126502. [CrossRef]
18. Yang, W.; Zhang, L. A multi-period intuitionistic fuzzy consensus reaching model for group decision making problem in social network. *Complex Intell. Syst.* **2024**, *10*, 7213–7234. [CrossRef]
19. Zhong, X.; Cao, J.; Yi, W.; Du, Z. Consensus reaching for large-scale group decision making: A gain-loss analysis perspective. *Expert Syst. Appl.* **2025**, *272*, 126742. [CrossRef]
20. Yu, Z.; Kou, J.; Liu, Y.; Chu, H. Decision algorithm with fuzzy framework and evaluation of advanced financial management policy. *Sci. Rep.* **2025**, *15*, 31184. [CrossRef] [PubMed]
21. Dombi, J.; Fáro, J.; Jónás, T. A fuzzy entropy-based group consensus measure for financial investments. *Mathematics* **2024**, *12*, 4. [CrossRef]
22. Xie, X.; Sathasivam, S.; Ma, H. An Interval-valued Intuitionistic Fuzzy Group Decision-making Approach Based on Projection Measurement Extended VIKOR for Patent Quality Evaluation. *PLoS ONE* **2025**, *20*, e0323019. [CrossRef]
23. Deveci, K.; Güler, O. Ranking intuitionistic fuzzy sets with a hypervolume-based approach: An application for multi-criteria assessment of energy alternatives. *Appl. Soft Comput.* **2024**, *150*, 111038. [CrossRef]
24. Atanassov, K.T.; Marinov, E. Four distances for circular intuitionistic fuzzy sets. *Mathematics* **2021**, *9*, 1121. [CrossRef]
25. Chen, T.Y. Evolved distance measures for circular intuitionistic fuzzy sets and a C-IF TOPSIS approach. *Artif. Intell. Rev.* **2023**, *56*, 7347–7401. [CrossRef]
26. Song, H.H.; Wang, Y.M.; Martínez, L. Enhancing group decision-making: Maximum consensus aggregation for fuzzy cross-efficiency under hesitant fuzzy linguistic information. *Comput. Ind. Eng.* **2024**, *197*, 110622. [CrossRef]
27. Arora, H.D.; Naithani, A.; Chanian, R. Similarity measures for q-rung orthopair fuzzy sets and applications to decision making. *Math. Found. Comput.* **2024**, *8*, 259–284. [CrossRef]
28. Wang, D.; Yuan, Y.; Liu, Z.; Zhu, S.; Sun, Z. Novel Distance Measures of q-Rung Orthopair Fuzzy Sets and Their Applications. *Symmetry* **2024**, *16*, 574. [CrossRef]
29. Rasool, Z.; Gurmani, S.H.; Niazi, S.; Zulqarnain, R.M.; Khalifa, H.A.E.W. An integrated CRITIC and EDAS model using linguistic T spherical fuzzy Hamacher aggregation operators and its application to group decision making. *Sci. Rep.* **2024**, *15*, 6122. [CrossRef]
30. Xu, Y.; Ju, Y.; Gong, Z.; Sun, J.; Dong, P.; Porcel, C.; Herrera-Viedma, E. A utility-based three-way group decision consensus model with overlapping subgroups. *Inf. Sci.* **2024**, *678*, 120904. [CrossRef]
31. Tanino, T. Fuzzy preference orderings in group decision making. *Fuzzy Sets Syst.* **1984**, *12*, 117–131. [CrossRef]
32. Herrera, F.; Herrera-Viedma, E. Linguistic decision analysis: Steps for solving decision problems under linguistic information. *Fuzzy Sets Syst.* **2000**, *115*, 67–82. [CrossRef]
33. Herrera-Viedma, E.; Herrera, F.; Chiclana, F.; Luque, M. Some issues on consistency of fuzzy preference relations. *Eur. J. Oper. Res.* **2004**, *154*, 98–109. [CrossRef]
34. Xu, Z.; Ren, P. A survey of decision making with hesitant fuzzy preference relations: Progress and prospect. *Syst. Eng. Theory Pract.* **2020**, *40*, 2193–2202. [CrossRef]
35. Únver, M. Gaussian Aggregation Operators and Applications to Intuitionistic Fuzzy Classification. *J. Classif.* **2025**, *42*, 595–623. [CrossRef]
36. Pratama, D.; Yusoff, B.; Abdullah, L.; Kilicman, A.; Kamis, N.H. Extension operators of circular intuitionistic fuzzy sets with triangular norms and conorms: Exploring a domain radius. *AIMS Math.* **2024**, *9*, 12259–12286. [CrossRef]

37. Dasan, M.A.; Bementa, E.; Aslam, M.; Little Flower, V.F. Multi-attribute decision-making problem in career determination using single-valued neutrosophic distance measure. *Complex Intell. Syst.* **2024**, *10*, 5411–5425. [CrossRef]
38. Alreshidi, N.A.; Shah, Z.; Khan, M.J. Similarity and entropy measures for circular intuitionistic fuzzy sets. *Eng. Appl. Artif. Intell.* **2024**, *131*, 107786. [CrossRef]
39. Shepard, R.N. Toward a universal law of generalization for psychological science. *Science* **1987**, *237*, 1317–1323. [CrossRef]
40. Gong, K.; Ma, W.; Lei, W.; Zhang, H.; Goh, M. An individual satisfaction and influence measure-based approach for multi-attribute large-scale group decision-making with uncertain linguistic preference relations. *Comput. Ind. Eng.* **2025**, *201*, 110888. [CrossRef]
41. Li, X.M.; Min, M.; Tan, C.F. The functional assessment of agricultural ecosystems in Hubei Province, China. *Ecol. Model.* **2005**, *187*, 352–360. [CrossRef]
42. Xu, Z. Intuitionistic preference relations and their application in group decision making. *Inf. Sci.* **2007**, *177*, 2363–2379. [CrossRef]
43. Jiang, G.; Song, A. Projection-based TOPSIS method to MAGDM in dual probabilistic linguistic information environment. *J. Intell. Fuzzy Syst.* **2024**, *46*, 4557–4572. [CrossRef]
44. Xu, Z.; Cai, X. On consensus of group decision making with interval utility values and interval preference orderings. *Group Decis. Negot.* **2013**, *22*, 997–1019. [CrossRef]
45. Xu, Z.; Chen, J. Some models for deriving the priority weights from interval fuzzy preference relations. *Eur. J. Oper. Res.* **2008**, *184*, 266–280. [CrossRef]
46. Xu, Z.; Yager, R.R. Dynamic intuitionistic fuzzy multi-attribute decision making. *Int. J. Approx. Reason.* **2008**, *48*, 246–262. [CrossRef]
47. Behret, H. Group decision making with intuitionistic fuzzy preference relations. *Knowl. Based Syst.* **2014**, *70*, 33–43. [CrossRef]
48. Chu, J.; Liu, X.; Wang, Y.; Chin, K.S. A group decision making model considering both the additive consistency and group consensus of intuitionistic fuzzy preference relations. *Comput. Ind. Eng.* **2016**, *101*, 227–242. [CrossRef]

Disclaimer/Publisher's Note: The statements, opinions and data contained in all publications are solely those of the individual author(s) and contributor(s) and not of MDPI and/or the editor(s). MDPI and/or the editor(s) disclaim responsibility for any injury to people or property resulting from any ideas, methods, instructions or products referred to in the content.